Spectroscopic Studies of Ionic Complexes and Clusters

E. J. Bieske* and J. P. Maier*

Institut für Physikalische Chemie der Universität Basel, Klingelbergstrasse 80, 4056 Basel, Switzerland

Received May 18, 1993 (Revised Manuscript Received August 5, 1993)

Contents

I.	Introduction	2603
II.	Aromatic Cation–Ligand Systems	2604
III.	Small Inorganic Cation–Ligand Systems	2607
IV.	Metal Cation–Ligand Complexes	2615
V.	Negative Ion Clusters	2618
VI.	Conclusions	2620

I. Introduction

Ionic clusters are ubiquitous in all gas-phase environments, being particularly abundant in plasmas, flames, and the terrestrial atmosphere[1,2] and are also likely constituents of the interstellar medium. Ion-induced dipole and ion–dipole forces result in bonded entities whose dissociation energies (100–5000 cm^{-1}) lie between those of van der Waals and fully chemically bound species. Besides possessing technological and environmental relevance, they serve as convenient systems to investigate liquid-phase structures surrounding a solvated ion. Despite this fundamental importance, it is only in the last 5–10 years that there have been successful attempts to harness the techniques of modern spectroscopy to explore ionic cluster structures. Hitherto efforts had focused more on measuring abundances in particular environments,[1] formation mechanisms, enthalpies and entropies of formation,[2,3] and reactivities.[4,5] While a certain amount of structural information can be inferred from these sorts of studies, it is from microwave, infrared (IR), and optical spectroscopy that one can in principle learn most. In 1986 Castleman and Keesee provided a commendable review of earlier work.[4] Since that time spectroscopic activities have flourished making a survey of recent results appropriate.

This review is primarily devoted to discussing the spectroscopic characterization of relatively weakly bound ionic complexes. It concentrates on results obtained for quite disparate chemical species including metal ions solvated by noble gas, water or inorganic molecular ligands, protonated hydrogen, ammonia and water complexes, inorganic molecular chromophores such as N_2^+ surrounded by rare gas atoms, and aromatic rings with one or more rare gas atoms attached. Different experimental groups have undertaken spectroscopic studies in the microwave, infrared, and visible regions. Although spectroscopic exploration of ionic complexes has been accomplished across the electromagnetic spectrum it appears that no single species has been observed in more than one spectral range. This is a measure of the field's infancy and is a situation that surely will not persist.

The relatively strong binding arising from charge-induced dipole forces ensures the existence of a variety of different clusters in any cool, ionized gas-phase environment. The blooming of cluster and complex ion spectroscopic investigations has paralleled the development of spectroscopic methods that permit the selective study of one particular component. The two most common methods have involved zero kinetic

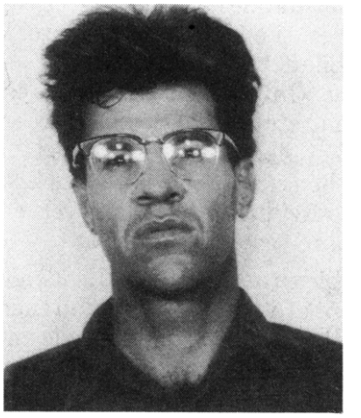

Evan Bieske was born in Mackay, Australia. He studied physics and mathematics at the University of Queensland and later (1989) obtained a Ph.D. under the supervision of Professor Alan Knight at Griffith University with work on the spectroscopy and dynamics of neutral and ionic aromatic–rare gas complexes. Since 1990 he has been engaged in the spectroscopic investigation of small ionic complexes in Basel, Switzerland.

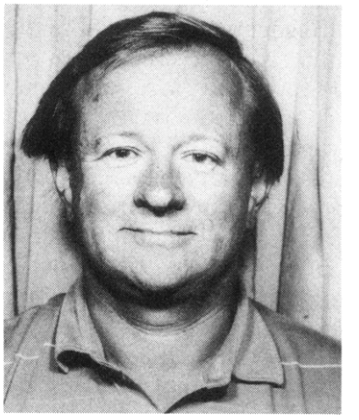

John P. Maier received a B.Sc. in chemistry at Nottingham University, U.K. (1969) and a D.Phil. in physical chemistry from Oxford University (1972) working under D. W. Turner. After a postdoctoral period with E. Heilbronner, he remained at his present address and was appointed to the chair of physical chemistry at Basel University in 1991. He was awarded the Werner prize of the Swiss Chemical Society (1979), Marlow medal of the British Chemical Society (1980), the Chemistry prize of the Akademie der Wissenschaften zu Göttingen, Germany (1986), and the Latsis prize of the Swiss Science Foundation (1987). His research interests lie in the development and application of methods for the spectroscopic characterization of ions, ionic clusters and radicals in the gas phase, and rare gas matrices.

0009-2665/93/0793-2603$12.00/0

energy photoelectron spectroscopy (ZEKE) and the use of mass spectroscopic methods for the preparation of a pure cluster population followed by resonant photodissociation. While conventional laser-excited fluorescence and microwave methods have been of some importance, most recent studies have exploited species selective techniques.

A review of the ZEKE method by Müller-Dethlefs and Schlag has recently appeared[6] and the interested reader should consult this for a comprehensive discussion of techniques and results. Briefly, the procedure involves the detection of zero kinetic energy electrons while a tunable ionizing light source is scanned in frequency. Only transitions which resonantly access ion rovibronic states and produce accompanying zero kinetic energy electrons are detected. The resolution of the method ($\sim$0.5 cm^{-1}) is such that for small molecules individual rotational levels can be observed using standard laser equipment.

In favorable situations ZEKE is ideally suited to the measurement of adiabatic ionization energies and hence cluster binding energies. Both single and multiphoton ionization are possible, the former having the advantage that one needs to consider only the ground states of neutral and cation and can forget the spectroscopy of intermediate states, although generation of the VUV light necessary for single photon ionization can be a problem and generally requires frequency tripling in either metal vapor or a rare gas cell or expansion. As well, with one-photon VUV ionization, all species present in the ionization volume are able to contribute to the spectrum, limiting the species selectivity of the technique. Resonance-enhanced multiphoton ionization on the other hand accesses the cation levels through intermediate rovibronic levels of the neutral complex, promoting species selectivity but requiring spectroscopic knowledge of the intermediate states of the neutral cluster. In many instances this is not a problem, as the vibronic structure of intermediate states is well understood. There are some instances where there are difficulties in employing ZEKE spectroscopy for the investigation of the ground states of ionic complexes, either because of unfavorable Franck–Condon factors linking the neutral and ionic vibronic states, or because the ground state of the neutral does not exist as a bound species. This latter situation pertains in the case of the odd-hydrogen cation cluster series (H_{2n+1}^+).

Resonance-enhanced photodissociation of mass-selected ions has been the most commonly practiced species-selective technique. Absorption of a photon whose energy is in excess of the cluster's binding energy can lead directly or indirectly to dissociation with subsequent efficient detection of the ionic fragment. When the absorbed photon is in the infrared vibrational predissociation can occur. If an electronic transition is excited dissociation can occur on the upper electronic surface or may follow fluorescence or internal conversion to lower electronic states. One problem occurring when absorption of light is inferred from cluster photodissociation is that spectral band intensities represent a convolution of absorption cross section and a state-dependent photofragmentation yield. Radiation may or may not be followed by dissociation depending upon the relevant Franck–Condon factors and dissociation energies.

Calculations of ionic structures and vibrational frequencies have been of some importance in assisting experimentalists to choose appropriate spectral ranges for their investigations and also in providing insights and geometries. Given their open-shell electronic structure and the dominant cohesive role of rather weak dispersion and induction forces, construction of accurate ab initio potential surfaces for ionic complexes is not an easy task. Moreover, the calculational difficulties do not end once a reliable potential energy surface has been obtained. Many ionic systems undergo large amplitude anharmonic motions with modest internal energies. While many determinations of rovibrational energies have used harmonic oscillator/rigid rotor approximations, general variational rovibrational calculations have been performed for several ionic triatomic systems.[7,8] The problem of large amplitude motions becomes more severe the larger the system, and to date there does not seem to be a general method for determining the rovibrational energy levels of systems with four or more atoms. One ionic system where such calculations would be particularly useful is H_5^+. Ab initio calculations show that barriers for nuclear rearrangement are small, rendering harmonic oscillator analyses of the vibrational motion suspicious.

The focus of this review is on spectroscopic studies that provide direct evidence to structure. We do not consider the considerable body of experimental and theoretical work concerned with bound-free electronic transitions in ionic complexes. Generally cation complexes consisting of two like moieties, one minus an electron, have one bound and one repulsive electronic state correlating with ground-state fragments. Although observation of transitions between these two states leads to limited structural information on the ground state of the complex, it is possible to determine binding energies and the symmetry of the transition by measuring the angular and kinetic energy distributions of the fragments. Further details of these types of studies can be found in ref 9. Conventional photoelectron spectroscopy and photoion studies of supersonic expansions of various gas mixtures have also been of importance in the determination of ionic complex properties but the limited resolution of these techniques means that they are incapable of providing direct structural information. A partial list of dimer and trimer systems studied by these and other means is given in Table I.

II. Aromatic Cation–Ligand Systems

A number of different aromatic cation–ligand complexes have been studied in the last few years; the activity due to the well-characterized spectroscopy of the neutral state of the aromatic core which facilitates preparation of cation complexes in well-defined vibrational levels using resonant multiphoton ionization (REMPI). Although studies of substituted benzene cations with rare gas atom ligands have been most common, complexes involving chemically more interesting ligands such as H_2O and CH_4 have also been investigated.

A. Benzene$^+$–Ar

The benzene$^+$–argon complex has been studied using ZEKE spectroscopy.[73] An increase in the rare gas–ring

Table I. Selected Dimer and Trimer Cation Binding Energies and Reference Sources

species	D_0 (ev)	ref(s)
He_2^+	2.475	10–12
Ne_2^+		13
Ne_3^+	0.11	14
Ar_2^+		13,15–17
Kr_2^+	1.176	13,15,18,19
Xe_2^+	1.02	13,18,20
$HeNe^+$	0.699	21–24
$HeAr^+$	0.026	21,22,25
$HeKr^+$	0.023	21,22,26
$HeXe^+$	0.042	22,26,27
$NeAr^+$		22,26,27
$NeKr^+$	0.055	26
$NeXe^+$	0.041	26
$ArKr^+$	<0.568	28,27
$ArXe^+$	0.179	28,29
$KrXe^+$	0.385	27,28
He_3^+	0.16	14,30
Ar_3^+	0.21	14,16,31–37
$(N_2)_2^+$	0.9	37–41
$(N_2)_3^+$		37,39,40
$(O_2)_2^+$	0.4	42,43
$CoAr^+$		44
CO_2^+Ar		45
O_2^+Ar		46
N_2Ar^+	1.07	37,47,48
$Ar_2N_2^+$		37,49
$NOAr^+$	0.129	50,51
$(H_2O)_2^+$		52
$(H_2S)_2^+$		53
$(H_2S)_3^+$		53
$(C_2H_2)_2^+$		54
$(C_2H_4)_2^+$	0.79	55
$(C_2H_4)_3^+$	0.182	56
$(C_6H_6)_2^+$		57–59
$(CO)_2^+$	0.97	39,60,61
$(CO)_3^+$		39,61
$(CO_2)_2^+$		62,63
$(CO_2)_3^+$	0.143	62,63
$(NO)_2^+$	0.598	39,64,65
$(N_2O)_2^+$	0.568	62
$(CS_2)_2^+$	0.759	66,67
$(OCS)_2^+$	0.746	68
$(SO_2)_2^+$	0.66	69
Hg_2^+		70
$HgAr^+$	0.228	71
$HgKr^+$	0.393	72
$HgXe^+$	0.748	72

binding energy of 172 ± 2.5 cm^{-1} is found to accompany ionization, although this increase in stabilization does not appear to be marked by large geometry changes as no intermolecular vibrations were observed in the spectrum.

B. Hexafluorobenzene$^+$–He_m Ne_m Ar_n

Miller and co-workers have undertaken extensive investigations of the hexafluorobenzene cation complexed with He,[74] Ne, and Ar[75] ligands using laser-excited fluorescence (LIF). Hexafluorobenzene, entrained in an inert gas expansion, is ionized by the output of an ArF excimer laser with subsequent clustering occurring around the ion seed. Although the LIF spectra contain contributions from clusters with various numbers of rare gas atoms, judicious adjustment of experimental conditions permits attribution of the various spectral peaks to clusters with a specific constitution.

As an example, Figure 1 shows the LIF spectrum obtained near the B ← X origin transition of $C_6F_6^+$ when C_6F_6 is expanded in pure helium.[74] All the weaker

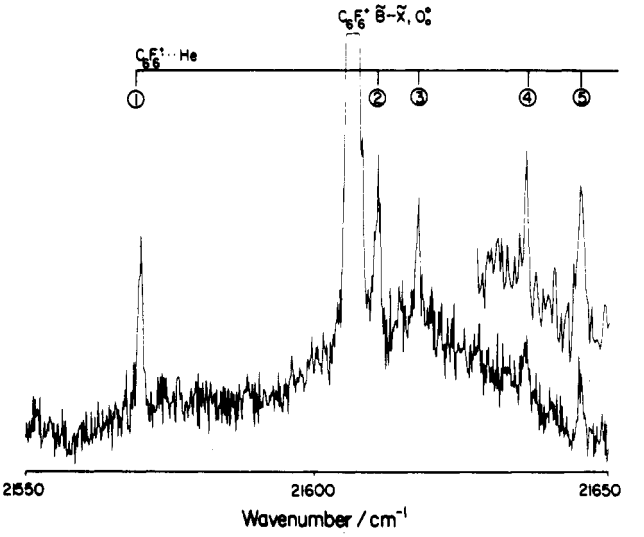

Figure 1. Fluorescence excitation spectrum close to the origin of the B ← X system of $C_6F_6^+$. The numbered lines (1–5) correspond respectively to the 0_0^0, s_0^1, b_0^2, b_0^4, and s_0^2 transitions of $C_6F_6^+$–He. The intensities are not proportional to the intrinsic oscillator strength as partial saturation exists. (Reprinted from ref 74. Copyright 1986 American Institute of Physics.)

bands in the spectrum are attributed to the $C_6F_6^+$–He complex. Vibrational energy levels have been calculated by first generating a potential energy surface in terms of atom–atom interactions with the inclusion of charge-induced dipole terms, followed by numerical solution of the Schroedinger equation. Band shifts for the $C_6F_6^+$–He and $C_6F_6^+$–He_2 species are reported as 38 and 81 cm^{-1}, respectively, the approximate proportionality between ligand number and electronic shift constituting evidence that the first two helium ligands bind in equivalent sites above and below the center of the aromatic ring.

Complexes formed with $C_6F_6^+$ and Ne[76] or Ar[75,77] ligands have also been studied using the LIF technique[76] although in these cases the spectra exhibit a profusion of lines due to the presence of many different cluster stoichiometries and structures, and to the activity of the low-frequency intermolecular vibrations accompanying the electronic transition making interpretation of the spectra less straightforward than it is for complexes involving He. With argon expansions, bands displaced by 420 and 785 cm^{-1} to the red of the $C_6F_6^+$ origin have been assigned as the origins of the $C_6F_6^+$–Ar and $C_6F_6^+$–Ar_2 complexes with the noble gas atoms positioned above and below the ring center.[77] For $C_6F_6^+$–Ne, the origin transition occurs 56 cm^{-1} to the red of the $C_6F_6^+$ origin.[76] At higher expansion pressures, the LIF spectra display extremely broad bands with no discrete features.

C. Aniline$^+$–Ar_n

Ionic complexes of aniline and argon (An^+–Ar and An^+–Ar_2) have been characterized using two color, resonant ionization ZEKE spectroscopy.[78,79] As in the corresponding neutral van der Waals molecules,[80] the geometry of the An^+–Ar complex appears to be such that the Ar atom occupies a position above the ring (C_s symmetry). For An^+–Ar_2 the argon atoms take up equivalent positions on opposite sides of the ring. Ionization through the S_1 state of the neutral results in

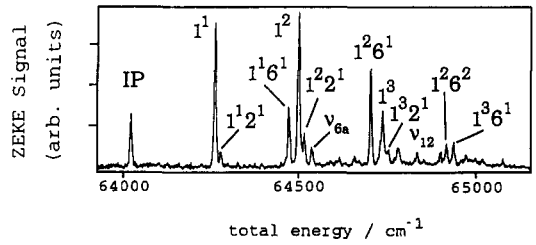

Figure 2. Two-photon two-color ZEKE spectrum of the phenol–H_2O complex obtained using the vibrationless S_1 state as an intermediate. Three intermolecular vibrational modes are active in the spectrum—ν_1 a hydrogen bond stretch mode (240 cm^{-1}), ν_2 an out-of-plane bend mode (18 cm^{-1}) only seen in combination with the stretch, and ν_6 an in-plane bend mode (203 cm^{-1}). (Reprinted from ref 82. Copyright 1992 VCH.)

long progressions in the symmetric bending coordinate, a consequence of the ionization affecting the nonbonding orbital on the nitrogen atom. The binding energy of An^+–Ar, inferred from the ionization potential and the binding energy of the neutral complex, is 510 cm^{-1}, marginally larger than the 400 cm^{-1} binding energy for the S_0 state of the neutral.[81]

The intermolecular vibrational frequencies observed for the ground state of the An^+–Ar and An^+–Ar_2 complexes are comparable to those of the neutral complexes in the S_1 state, demonstrating that removal of a single electron in a system as large as aniline has a relatively minor effect on its interaction with a rare gas atom whose ionization potential is much higher. Although ionization increases the stretching s_z frequency from 49 to 66 cm^{-1}, the b_x bending frequency actually *decreases* from 22 to 15 cm^{-1}, a phenomenon attributed to the flattening of the potential along this coordinate due to competition between ion-induced dipole forces that attract the argon toward the nitrogen atom and dispersion forces that encourage it to stay above the ring.[79] For An^+–CH_4 a binding energy of around 570 cm^{-1} has been deduced, a modest increase compared to the corresponding neutral van der Waals molecule (S_1 state D_0' = 480 cm^{-1}; S_0 state D_0'' = 400 cm^{-1}).[79] The only progression apparent in the ZEKE spectrum has a spacing of around 20 cm^{-1} and has been assigned to the b_x bending vibration.

D. Phenol$^+$–H_2O

Pronounced interactions between an ionized aromatic and ligand occur in the phenol$^+$–H_2O system.[82,83] Ionization of the neutral complex results in the formation of an ion–dipole bond, with a consequence increase in the binding energy of the complex by 602 cm^{-1} and significant geometrical rearrangements. The ZEKE spectrum of phenol$^+$–H_2O shown in Figure 2 exhibits activity in three intermolecular modes—a hydrogen bond stretch mode (240 cm^{-1}), an out-of-plane bend mode (18 cm^{-1}) only seen in combination with the stretch and an in-plane bend mode (203 cm^{-1}).

E. Fluorobenzene$^+$–Ar, Chlorobenzene$^+$–Ar, and Paradifluorobenzene$^+$–Ar

Electronic transitions in the fluorobenzene–argon (FB^+–Ar) and chlorobenzene–argon (CB^+–Ar) cation complexes have been studied by monitoring laser-induced photodissociation following excitation of the B ← X transition.[84] The ground-state ions were created by resonance enhanced multiphoton ionization (REMPI) of the neutral van der Waals molecules via the neutral S ← S_0 transition. Unfortunately this means of ionization delivers substantial energy into the vibrations of the complex, and subsequently obtained resonance-enhanced photodissociation spectra are marked by considerable congestion due to closely spaced sequence transitions. While assignment of transitions involving the high-frequency ring vibrations was possible, it was difficult to unravel the dense structure associated with the intermolecular motions.

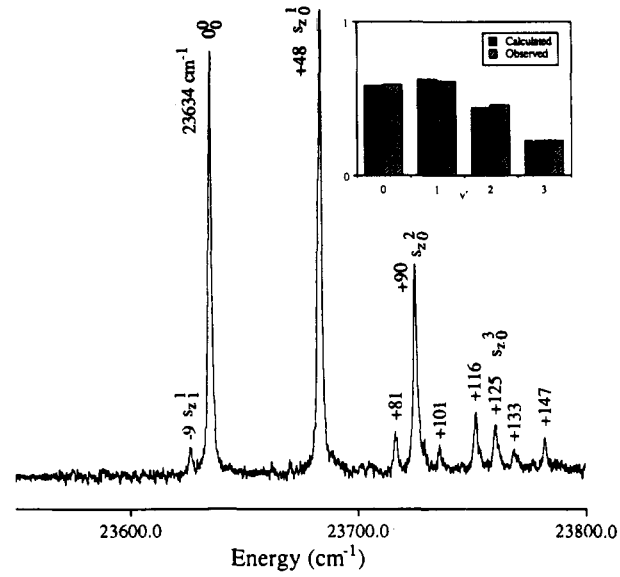

Figure 3. Photodissociation spectrum of the $pdFB^+$–Ar cation complex in the 423-nm region. The dominant vibrational structure corresponds to a progression in the Ar···$pdFB^+$ stretching vibration. Band displacements are shown relative to the complex 0_0^0 transition at 23 634 cm^{-1}. Inset: Comparison of calculated Franck–Condon intensities with those observed for the parameters δ = 1.09 and D = 1.52. (Reprinted from ref 85. Copyright 1990 American Institute of Physics.)

The difficulties due to the creation of internally excited complexes were circumvented in an ensuing study of the paradifluorobenzene$^+$–Ar ($pdFB^+$–Ar) complex.[85,86] Resonant two-photon ionization through the S_1 ← S_0 transition of the neutral van der Waals molecule was employed to create the ground-state ionic complexes. For pdFB–Ar, the energy of the S_1 ← S_0 transition is almost exactly half the ionization energy, so that vibrationally quiescent $pdFB^+$–Ar cations can be produced using one-color, two-photon ionization. Well-structured bands involving the low-frequency intermolecular stretching and bending motions were observed when the second laser was scanned in the 423-nm region. Figure 3 shows the spectrum, giving assignments and a comparison of observed and calculated line intensities assuming that the dominant progression is due to the intermolecular ring–argon stretching motion. The spectra are consistent with a structure where the Ar atom is positioned over the middle of the ring (C_{2v} symmetry). In the excited electronic state of the ion, the intermolecular stretch vibration has a frequency of 48 cm^{-1} compared to 41 cm^{-1} for the neutral van der Waals molecule,[87] the increase reflecting the additional attraction resulting from charge-induced dipole forces. A Franck–Condon analysis (Figure 3 inset) indicates a change of 0.2 Å in the Ar···$pdFB^+$ bond distance accompanying electronic excitation. Spectra obtained for the $pdFB^+$–Ar_2 complex show that the two Ar···$pdFB^+$ bonds are equivalent

and have approximately the same stretching force constant as in pdFB$^+$–Ar$_1$.

F. *p*-Dimethoxybenzene$^+$–Ar$_n$ Complexes

The *cis* and *trans* isomers of the *p*-dimethoxybenzene$^+$–Ar$_n$ (n = 1, 2) complexes have been investigated using two-color resonant ZEKE spectroscopy.[88] Quite different vibrational structures were observed for the two isomers. Conspicuous in the *p*-dimethoxybenzene$^+$–Ar$_1$ spectra are bands resulting from excitation of the intermolecular stretching vibrations—43 cm^{-1} for the *cis* and 47 cm^{-1} for the *trans* isomer.

G. Phenylacetylene$^+$–Ar and Styrene$^+$–Ar

The ground electronic states of the phenylacetylene$^+$–Ar and styrene$^+$–Ar complexes have been studied using ZEKE spectroscopy.[89] Binding energies of 554 ± 10 cm^{-1} for phenylacetylene$^+$–Ar and 512 ± 26 cm^{-1} for styrene$^+$–Ar can be compared to the neutral (S_0 state) binding energies of 406[90] and 396 ± 16 cm^{-1},[91] respectively. As in the case of aniline–Ar, the ZEKE spectrum of both species displays a 15-cm^{-1} progression arising from excitation of the low-frequency bending mode (a′ symmetry) accompanying ionization.

H. Phenol$^+$–Trimethylamine

The wavelength-dependent photodissociation spectrum of (phenol–trimethylamine)$^+$ has been obtained in the 350–430-nm range by monitoring the HN(CH$_3$)$_3^+$ photoyield.[92] The complex is prepared using REMPI of the neutral complex, a process that essentially removes an electron from the phenol moiety. The spectrum is similar to solution absorption spectrum of the phenoxy radical prepared by pulse radiolysis, suggesting a ground-state structure for the ion more akin to a phenoxy radical–trimethylammonium (C$_6$H$_5$O–H$^+$N(CH$_3$)$_3$) structure. Because the ionization process does not access the vibrational ground-state of the complex, subsequently probed molecules are likely to have considerable internal energy accounting for the broad peaks observed in the spectrum.

I. Benzene Dimer and Trimer Cations

Photoabsorption by the benzene dimer, trimer, and tetramer cations have been investigated by monitoring the wavelength-dependent photodissociation yield of $C_6H_6^+$ in the 410–750-nm range.[57,93] Cation clusters were prepared using nonresonant MPI at 210 nm of benzene clusters formed in a mixed argon and benzene supersonic expansion and were dissociated in the source region of a reflection time of flight mass spectrometer. Multiphoton ionization at 210 nm possibly imparts considerable internal energy to the cation complexes leading to broad bands in the cation spectrum. For both the dimer and trimer cations only $C_6H_6^+$ fragments were observed, though the tetramer yielded both $C_6H_6^+$ and $(C_6H_6)_2^+$ fragments. Two broad bands centered at 440 and 580 nm in the dimer spectrum (Figure 4) have been assigned respectively to the $A_{2u} \leftarrow E_{1g}$ and $E_{2g} \leftarrow E_{1g}$ transitions localized on $C_6H_6^+$. Transitions that would be symmetry forbidden in the monomer are allowed in the dimer because of its lower symmetry. Further photodissociation signal extending into the near IR is probably due to an intravalence transition common

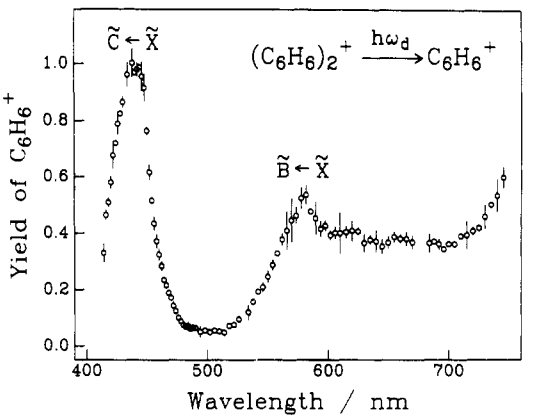

Figure 4. Photodissociation spectrum (plots of the photofragment ion yield against laser wavelength) of the benzene cation dimer [$(C_6H_6)_2^+$] between 400 and 700 nm. The $C(A_{2u}) \leftarrow X(E_{1g})$ and $B(E_{2g}) \leftarrow X(E_{1g})$ transitions localized on $C_6H_6^+$ are labeled. (Reprinted from ref 57. Copyright 1991 American Institute of Physics.)

to most cationic homodimers. Measurements of the fragment kinetic energy after excitation into the 440-nm band suggests that the transition is to a bound state.[59] The trimer cation exhibits similar spectral structure to the dimer though the $E_{2g} \leftarrow E_{1g}$ band is shifted to 620 nm. There have been other studies on the photodissociation of benzene cation clusters concerned more with the fragmentation patterns for the larger cluster.[93,58]

III. Small Inorganic Cation–Ligand Systems

A. N_2^+–He$_n$ and N_2^+–Ne$_n$

Because of its strong 390-nm B $^2\Sigma_u^+ \leftarrow$ X $^2\Sigma_g^+$ transition, N_2^+ serves as convenient chromophore to which one or more noble gas ligands can be attached.[94-96] While the electronic structure of the N_2^+ core is mildly perturbed for He and Ne adducts, when the ionization potential of the rare gas is close to that of N_2, e.g. N_2Ar^+, the complex has considerable charge-transfer character and can exhibit electronic transitions that are intrinsic to neither of its constituents but which are characteristic of the species as a whole.[37]

Photoabsorption of N_2^+–He$_n$ complexes has been investigated by monitoring resonant photodissociation in a quadrupole–octopole–quadrupole apparatus.[94,95-97] Twin electron beams emanating from two filaments positioned close to a nozzle orifice serve to ionize N_2 molecules in the initial region of a supersonic expansion (N_2/He ratio 1:1000, stagnation pressure 4 bar) either through Penning or direct ionization. Clusters are extracted from the expansion region through a skimmer/electrostatic lens assembly and focused into the first quadrupole where primary mass filtering of the desired cluster occurred. After leaving this quadrupole the ion beam is deflected through 90° by an electrostatic quadrupole bender and injected into an octopole ion trap where interaction with the pulsed laser beam occurs. The second quadrupole mass filter is tuned to transmit N_2^+ fragments resulting from photodissociation.

In Figure 5 the observed electronic spectrum of N_2^+–He$_n$ (n = 1–3) in the 390-nm region is reproduced. Structure in the N_2^+–He$_1$ spectrum resembles the rotational structure of the $B^2\Sigma_u^+ \leftarrow X^2\Sigma_g^+$ transition of

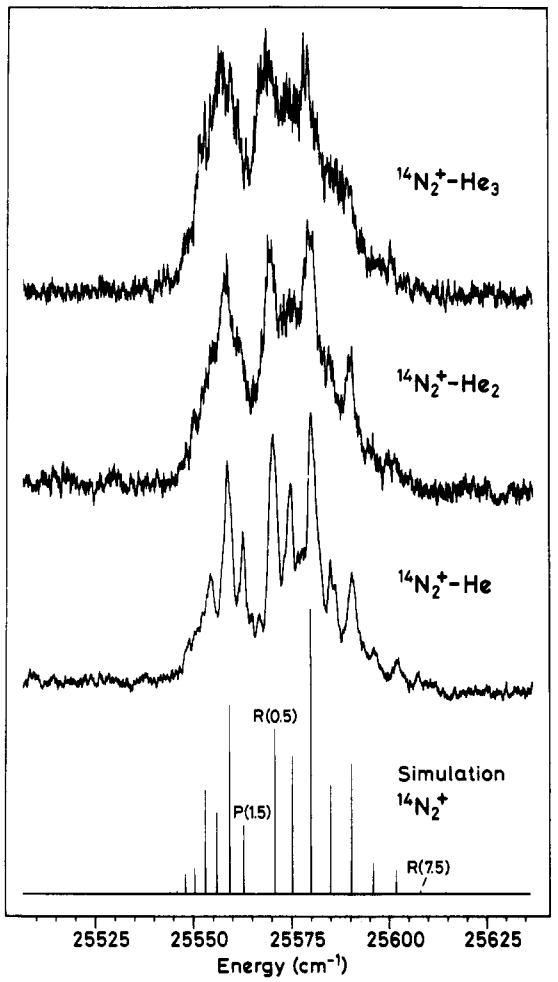

Figure 5. The B ← X electronic spectra of the N_2^+–He$_n$ (n = 1–3) complexes in the 390-nm region along with a simulation of the free N_2^+ spectrum at 30 K. Spectra are obtained by mass selecting the N_2^+–He$_n$ complexes and detecting the N_2^+ photodissociation product. The similarity of the N_2^+–He$_n$ spectra and the N_2^+ simulation is taken as evidence for free internal rotor structure for the complexes.

N_2^+ at a rotational temperature of 20–30 K (shown in the bottom part of the figure). Of note is the 2:1 intensity alternation, a consequence of the equivalence of the N atoms in the complex and the nuclear spin of ^{14}N (I = 1). When analogous measurements are carried out on $^{15}N_2^+$–He, the spectrum reveals instead a 1:3 intensity pattern due to the $I = {}^1/_2$ nuclear spin of $^{15}N_2$. Both "T"-shaped or "free" internal rotor structures, where the He does not have a well-defined angular location, are consistent with equivalent N atoms. Simulation of the band profile excludes the possibility that the structure of the N_2^+–He cluster is T-shaped; the conclusion is that there is free internal rotation of the N_2^+ moiety in both the X and B states. This is in accord with ab initio and rovibrational calculations undertaken for this complex in which the zero-point energy was found to be above the barrier for internal rotation.[8] The band profile of N_2^+–He arises chiefly from ±1 changes in the quantum number pertaining to the internal rotation of the N_2^+ core.

The band origin of N_2^+–He is shifted by merely ~1 cm^{-1} from that of N_2^+, indicating almost identical binding energies in the X and B states, consistent with the absence of any discernible progression in the He···N_2^+ stretching vibration in the spectrum. Furthermore, from the breaking off in the internal rotational structure in the R-branch (at j = 7), a lower estimate for the dissociation energy of N_2^+–He of 100–130 cm^{-1} may be inferred, comparable with the calculated X state D_0 value of ~98 cm^{-1}.[8]

The B ← X electronic transition of the cluster ions N_2^+–He$_n$, n = 2–6 have also be observed.[96] For the species with n = 2 and 3 the spectra (Figure 5) show similar features to that of n = 1, supporting the notion that free internal rotation persists with several helium atoms attached. Similar structure occurs for clusters with up to six He atoms, the largest cluster for which spectra have been recorded. It can be seen that as for the n = 1 case, the R-branch extends to the same point for $n \geq 2$, suggesting similar binding energies for additional He atoms (~100 cm^{-1}). This seems reasonable if one considers that binding of He atoms should be dominated by interactions with the N_2^+ core, with He–He interactions making a minor cohesive contribution.

Spectra of N_2^+–He display a hot band due the B ← X (1–1) transition, displaced ~195 cm^{-1} to higher energy from the origin band.[98] Initially the observation of the hot band is surprising as it is evidence that N_2^+–He (v = 1) complexes with energy far above the dissociation limit survive the 100–300-μs journey from source to octopole ion guide. The vibrational predissociation lifetime of N_2^+–He in the (v = 1) level has been determined as 220 ± 30 μs by measuring the relative intensities of the origin band and the hot band as the flight time from the ion source to the octopole is varied by changing electrical potentials in the machine.[98] The relatively slow rate of decay for N_2^+–He (v = 1) reflects the adiabatic decoupling of the fast N–N stretching vibration from the slower He···N_2^+ intermolecular motion. Dissociation requires that considerable energy be deposited into the relative translational motion of the fragments and/or N_2^+ rotation with correspondingly large changes in the effective quantum numbers for these two motions.

The first recorded observation of a transition in an N_2^+–Ne$_n$ complex was by David et al. who observed bands due to the B ← X (1–0) transition of N_2^+–Ne$_4$ and N_2^+–Ne$_5$ by recording photofragment intensities as a function of wavelength.[99] Their experiment, carried out in a triple quadrupole apparatus, employed an ion source consisting of a solid matrix of N_2 in Ne bombarded by an Ar^+ beam. Subsequently the B ← X spectra of the N_2^+–Ne$_n$ ($n \leq 8$) series were obtained near the 390-nm B ← X origin band system by the Basel group, using the same approach as for the N_2^+–He$_n$ studies.[95]

Fits of the rotational profile of the origin band (band b in Figure 6) lead to the conclusion that the N_2^+–Ne complex is probably quasilinear in the X and B states, with a decrease in the Ne···N_2^+ bond of 0.1 Å accompanying excitation into the B state.[95] The vibrational structure apparent in the lower segment of Figure 6 corresponds to progression, sequence, and combination bands involving the low-frequency van der Waals type modes. Thus, for example, the Ne···N_2^+ stretching mode has a frequency of ~104 cm^{-1} (band b to band h spacing in Figure 6) in the B state. The bands labeled c, d, e, f, and g are due to hot bands of the bending vibration, their shift to higher energy from the origin indicating a complex stiffer in the B than the X state. As the

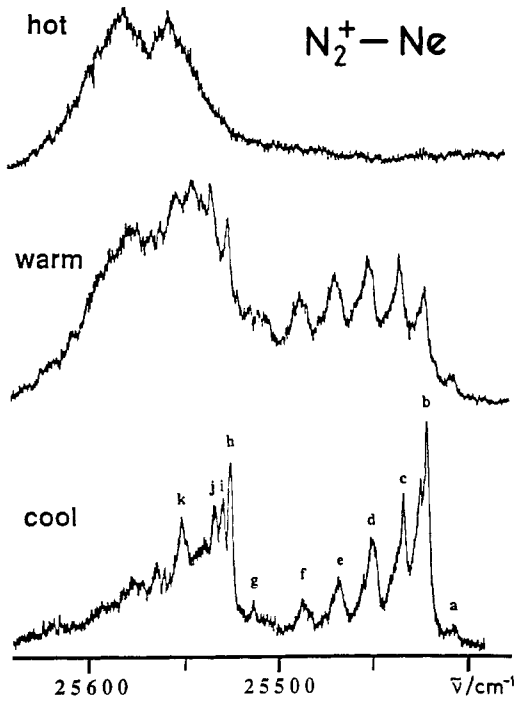

Figure 6. The B ← X electronic spectrum of N_2^+–Ne in the 390-nm region. The N_2^+–Ne complexes responsible for the three spectra have different effective temperatures as indicated by the labels. Band assignments are discussed in the text.

temperature is increased (middle segment of Figure 6), higher lying vibrational levels in the X state, more like the free internal rotor levels observed in N_2^+–He are populated. The profile at the highest temperature (upper segment of Figure 6) then comes to resemble that of N_2^+.

The spectroscopic studies of N_2^+–Ne complement those on the isoelectronic neutral species CN–Ne,[100] where the intermolecular potential energy surface has a decided linear minimum with a barrier of around 17 cm^{-1} to internal rotation in the X state, although it was impossible from the experimental data to decide whether a CN–Ne or an NC–Ne structure was preferred. In contrast to the N_2^+–Ne system there appears to be very little change in either the angular or radial form of the intermolecular potential accompanying B ← X electronic excitation.

B. N_2O^+–Ne and N_2O^+–Ar

Similar experimental techniques as used for the N_2^+–He_n and N_2^+–Ne studies were used to investigate the N_2O^+–Ne complex.[101] The situation is complicated by the fact that the ground state of the N_2O^+ ion core possesses orbital angular momentum ($^2\Pi$ ground state). An off-axis perturber mixes the $^2\Pi_{3/2}$ and $^2\Pi_{1/2}$ spin–orbit components to produce substates of A′ and A″ symmetries, the lower lying of which is expected to be preferentially populated among the ions produced by a supersonic source. The N_2O^+–Ne complex was formed (with an effective temperature of ~30 K) in the same manner as the N_2^+–He_n and N_2^+–Ne_n complexes, and the A ← X electronic spectrum was detected when the N_2O^+ product ion was monitored.[101] The most prominent peak in the spectrum is due to transitions from the lower electronic substate, while a smaller band shifted to lower energy by 141 cm^{-1} arises from

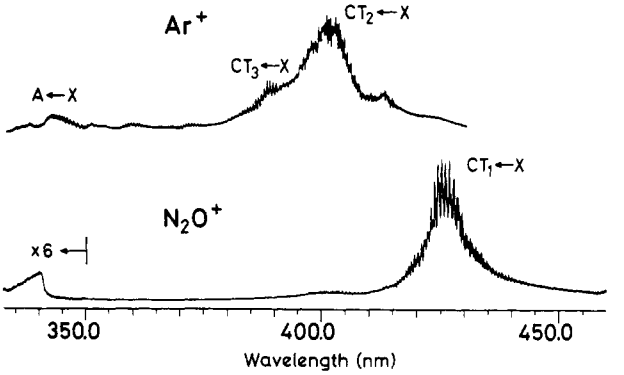

Figure 7. Spectra of the N_2O^+–Ar complex, extending from 450 nm down to below 335 nm, recorded by monitoring the N_2O^+ and Ar^+ fragment yield as the laser wavelength was scanned. The prominent bands between 380 and 450 nm arise from charge-transfer transitions while the weaker bands between 330 and 350 nm are due to an A ← X transition localized on the N_2O^+ moiety. See text for further discussion of band assignments.

transitions from the upper substate. The splitting between the A′ and A″ states is given by $(A_{so}^2 + \epsilon^2)^{1/2}$ where A_{so} is the spin–orbit coupling constant of X state N_2O^+, with the ordering of the A′ and A″ states depending on the sign of the interaction parameter ϵ. From the observed splitting and the previously determined value for A_{so} = 133.2 cm^{-1}; a $|\epsilon| = 50 \pm 8$ cm^{-1} can be deduced. A nonzero ϵ value implies a nonlinear geometry for N_2O^+–Ne.

The shift of the origin band for the cluster ion is 33 cm^{-1} to the blue from the monomer, in line with shifts in this energy direction observed for Σ–Π transitions of ions embedded in neon matrices. Whereas for the lowest and $\nu_2 = 1$ (NNO bend) levels of the A state of N_2O^+–Ne, only N_2O^+ fragment ions are produced, for the $\nu_1 = 1$ (NNO stretch) level, both N_2O^+ and a small fraction NO^+ ions are observed.

The N_2O^+–Ar complex differs from N_2O^+–Ne, in that the ionization potentials of its two constituents are separated by only ~2.9 eV suggesting that the complex should have considerable charge-transfer character.[97] Spectra of the N_2O^+–Ar complex in the ~450–335-nm range, recorded on both the Ar^+ and N_2O^+ mass channels, are shown in Figure 7.[97] As the ~435 nm onset of the system corresponds approximately to the difference in the ionization potentials of N_2O (12.89 eV) and Ar (15.76 eV), one is encouraged to suppose that the bands arise from intracluster photoinduced charge-transfer transitions between a ground state where the positive charge is localized principally on the N_2O, to states where the charge resides on the Ar. The broad bands are in fact composed of extensive overlapping vibrational progressions with spacings of the order of 50 cm^{-1} implying considerable rearrangement of the Ar···N_2O bond accompanying the electronic excitation.

The bands centered at 435, 401, and 387 nm (Figure 7) probably derive from transitions between the X state and the three charge-transfer states (CT_1, CT_2, and CT_3), expected to originate from the N_2O [$X^1\Sigma^+$] + Ar^+ [^2P_J] ($J = {}^1/_2, {}^3/_2$) limits. The general form of the wavelength-dependent photodissociation cross section and the Ar^+/N_2O^+ branching ratios are explicable in terms of several predissociation processes. At the onset of the first band (labeled CT_1 ← X in Figure 7),

photofragmentation to produce Ar^+ is energetically impossible; however, production of N_2O^+ may result from post fluorescence vibrational predissociation on the X state surface. Such a process accounts for the spectral features observed on the N_2O^+ mass channel between 445 and 415 nm. At higher energies, vibrational predissociation on the CT_1 surface to produce Ar^+ ($^2P_{3/2}$) becomes possible; sufficient vibrational energy is deposited in the CT_1 manifold for vibrational predissociation to occur before fluorescence.

From the ionization potentials of Ar and N_2O and onset energy for N_2O^+ and Ar^+ photoproduction, it is possible to estimate a binding energy of 650 cm^{-1} for the X state and 1340 cm^{-1} for the CT_1 state of the ionic complex. At 342 nm there is a sharp increase in N_2O^+ photoproduction that complements a reduction in Ar^+ signal. This is presumably due to rapid vibrational predissociation (vp) on the A-state potential energy surface producing N_2O^+ in the A state:

$$N_2O^+\text{–Ar}\ [X] + h\nu \rightarrow N_2O^+\text{–Ar}\ [A:\ E_{vib} > D_o'] \xrightarrow{vp} N_2O^+\ [A^2\Sigma^+] + Ar\ [^1S_0]$$

The $A \leftarrow X\ 1_0^1$ transition of the N_2O^+ monomer occurs at 338 nm, and the corresponding transition in N_2O^+–Ar is probably responsible for the production of N_2O^+ between 342 and 335 nm.

C. $(CO)_2^+$

The $(CO)_2^+$ ionic homodimer stands apart from most similar species in that it does not exhibit a broad unstructured dissociative absorption band in the visible or near UV region due to an intravalence transition.[9,60] Instead its wavelength-dependent photofragmentation spectrum displays a long, well-resolved progression (spacing of 470–490 cm^{-1}), tentatively assigned to a torsional or bending mode, beginning at around 310 nm and extending at least as far down as 270 nm.[60] It appears that $(CO)_2^+$ has an unusual ground-state geometry. According to ab initio calculations it has a C_{2h} symmetry with adjacent carbon atoms and a rather short C–C bond (r_{C-C} = 1.58 Å).[102] Transitions from a geometry with such a short C–C bond access the intravalence repulsive curve at much higher energy than is usual for these types of homodimers, hence the absence of visible absorption. The nature of the predissociative excited state probed in these experiments remains uncertain.

D. $(NO)_2^+$

The vibrational structure of the NO dimer cation has been studied using the ZEKE technique.[65] Ionization of the dimer was by way of a nonresonant one-color, two-photon process. The neutral NO dimer has been well characterized using microwave,[103] Raman, and infrared spectroscopies.[104] It has a planar *cis* structure (C_{2v}), adjacent N atoms and structural parameters: r_{N-N} = 2.33 Å, r_{N-O} = 1.15 Å, bonding angle ϕ = 95°, and $-\Delta H_f$ = 787 cm^{-1} (see inset to Figure 8b). Ionization increases the binding energy of the dimer by 4192 cm^{-1} and leads to a substantial change in the geometry, as evidenced by progressions in the low-frequency vibrational motions apparent in the ZEKE spectrum (Figure 8a). The 118-cm^{-1} progression has been assigned to an out-of-plane a_2 mode implying that the dimer ion has a nonplanar C_2 geometry.[65] The pattern of bands observed near the origin is repeated 2090 cm^{-1} higher (Figure 8b), corresponding to an excitation of the N–O bond stretch vibration. The 2090-cm^{-1} band lies between the NO and NO^+ stretch frequencies (1876 and 2344 cm^{-1}, respectively), suggesting that in the dimer cation, the charge is shared between the two NO constituents. There should in fact be two high-frequency stretching motions in the complex, corresponding to in-phase and out-of-phase deformation of the N–O bonds. The activity of only one vibration in the ZEKE spectrum is consistent with a structure where the two N–O bonds are equivalent in upper and lower states and where excitation of only the symmetric combination accompanies ionization.

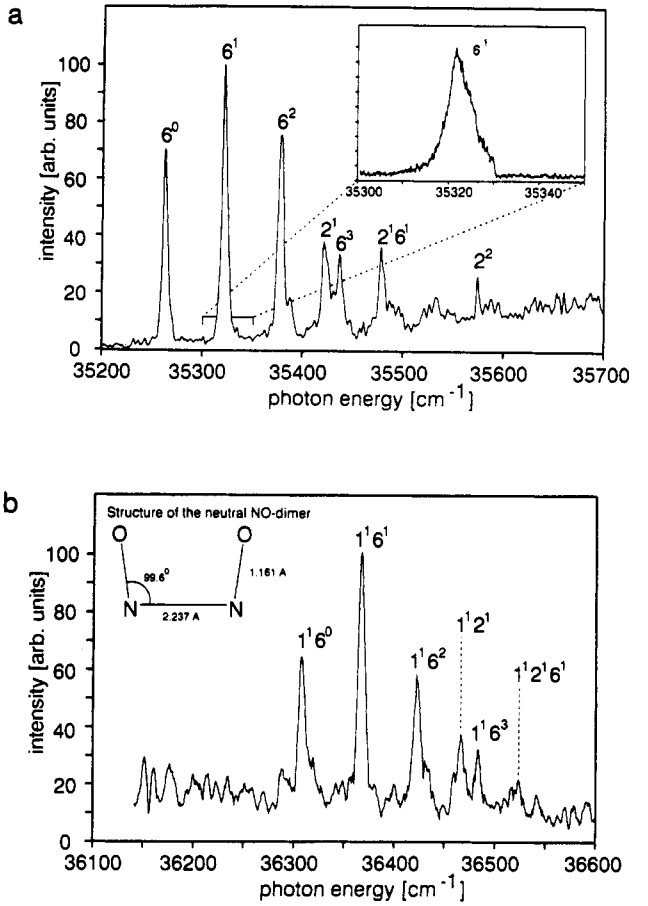

Figure 8. (a) Nonresonant two-photon ionization ZEKE electron spectrum of the NO dimer, $(NO)_2$. Tentative assignments of the peaks refer to a comparison with the neutral $(NO)_2$ modes known from earlier IR and Raman studies (ref 104). The inset shows a high accuracy scan of the rotationally broadened 6_0^1 band. (b) Same as a but at higher photon energy. The vibrational band pattern is repeated but shifted by 2090 cm^{-1} in total energy indicating NO stretch excitation in the $(NO)_2^+$. The inset shows the well-known structure of neutral $(NO)_2$. (Reprinted from ref 65. Copyright 1992 American Institute of Physics.)

E. NO^+–Ar

The applicability of the ZEKE technique to smaller atom–diatom ionic complexes is underlined by the Takahashi's recent studies of the NO^+–Ar complex[51] where ionization was accomplished with a 2 + 1 REMPI process:

Table II. Geometrical Parameters for NO–Ar and NO^+–Ar

state[a]	r_{N-O} (Å)	r_{N-Ar} (Å)	O–N–Ar (deg)
Ar–NO $X\ ^2\Pi_{1/2}$	1.15077[c]	3.711[c]	80.483[c]
Ar–NO $C\ ^2\Pi$	1.062	2.94	80.5
$(Ar–NO)^+\ X\ ^1\Sigma^+$	1.06322[d]	2.68[d]	69.2[d]

[a] The electronic states are denoted by analogy with those of NO. [b] Reference 106. [c] Reference 105. [d] Reference 51.

$$Ar–NO\ (X^2\Pi_{1/2}\ v'' = 0) + 2h\nu_1 \rightarrow$$
$$Ar–NO^*\ (C^2\Pi_{1/2}\ v' = 0) + h\nu_2 \rightarrow Ar–NO^+\ (X^1\Sigma^+ v^+)$$

Measurement of the adiabatic ionization potential allowed a binding energy of 951 cm^{-1} to be established for the ion ground state, considerably more than the neutral complex binding energy of 98 cm^{-1}.[105] Two strong progressions with spacings of 79 and 94 cm^{-1}, corresponding to the bending and stretching vibrations of NO^+–Ar are apparent in the spectrum. Although rotational structure was not resolved, a Franck–Condon analysis together with the neutral geometry known from microwave studies[105] yielded the structural parameters for the cation ground state (Table II).

F. Hydrogen Cluster Ions

The positive hydrogen cluster ions constitute the most fundamental series of protonated clusters and have attracted considerable experimental and theoretical attention. It has been found that the even H_{2n}^+ and odd H_{2n+1}^+ series have distinct properties;[107,108] however, as ion sources preferentially produce the odd series, spectroscopic attention has concentrated on them. Formation of the odd cluster series begins with the exothermic association reaction:

$$H_2^+ + H_2 \rightarrow H_3^+ + H$$

and continues with further H_2 additions. The enthalpies for the reactions

$$H_{2n+1}^+ + H_2 \rightarrow H_{2n+1}^+\ (n = 2–5))$$

have been measured by a number of groups,[109–114] with values for $n = 2$ ranging between 1750 and 3400 cm^{-1}, $n = 3$ between 630 and 1435 cm^{-1}, and the single determinations for $n = 4$ and $n = 5$ giving 1330 and 840 cm^{-1} respectively. A possible role for H_5^+ in interstellar chemistry has been suggested and in recent experiments an upper limit for the radiative association rate of H_3^+ and H_2 has been established.[115]

Calculations of binding energies and equilibrium geometries for the odd hydrogen cluster ions indicate that the smaller H_{2n+1}^+ clusters may be considered as an equilateral triangle H_3^+ unit, with H_2 molecules bound first to the apices of the triangle (for the first three H_2 units) and for larger clusters, above and below the triangle (see Figure 9).[116–121] It seems that H_5^+ deviates from this simple picture; the CI calculations performed by Yamaguchi et al. suggest that barriers in the potential energy surface for the rearrangement of nuclei are low.[120] The D_{2d} barrier for the H_3^+–H_2 ↔ H_2–H_3^+ isomerization is calculated to lie only 30 cm^{-1} above the potential minimum and in fact four stationary points on the H_5^+ potential hypersurface have been identified which lie within 1 kcal/mol of the minimum.[120]

Two experimental groups have studied the wavelength-dependent dissociation of hydrogen cluster ions.

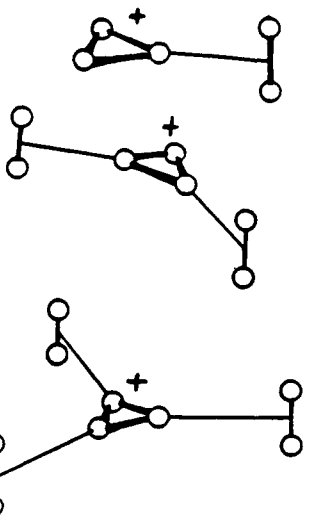

Figure 9. Sketch of H_n^+ (n = 5, 7, 9) cluster ions based on ab initio predicted geometries. (Reprinted from ref 123. Copyright 1988 American Institute of Physics.)

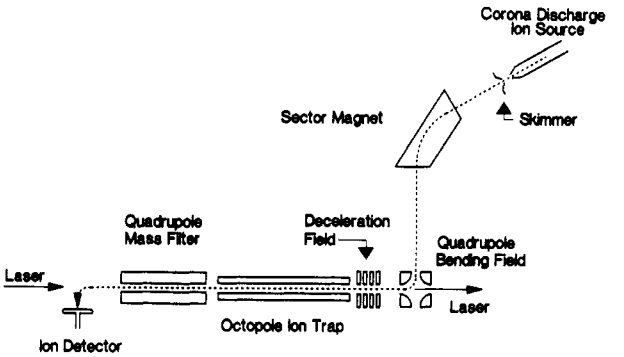

Figure 10. Experimental arrangement for the observation of the IR photodissociation of mass-selected cation clusters. Cluster ions produced by the ion source are mass selected by the magnetic sector before being deflected by 90° and introduced into an octopole ion guide where the laser/ion interaction occurs. Fragment ions are transmitted by a quadrupole mass filter and are eventually detected by a Daly scintillation detector. (Reprinted from ref 151. Copyright 1991 American Chemical Society.)

Okumura, Yeh, and Lee have recorded spectra of $(H)_n^+$ ($5 < n < 15$) between 3000 and 4200 cm^{-1}, a region that is expected to include the H_3^+ symmetric stretch and the H_2 stretch vibrations.[122,123] Bae on the other hand, has searched for wavelength-dependent dissociation of H_5^+ between 5400 and 10 000 cm^{-1} where overtone and combination bands are to be expected.[124]

It is worth pausing at this point to discuss the experimental arrangement employed by Okumura, Yeh, and Lee, as the same equipment has been used in the study of several other cluster systems, including the protonated ammonia and protonated water cluster ions discussed below. An overview of their apparatus is shown in Figure 10. In a typical experiment, H_{2n+1}^+ clusters are produced either by electron impact of neutral clusters formed in a continuous supersonic expansion (20–30 bar of pure H_2, 10 μm nozzle),[122] or with a corona discharge supersonic source[123] of a type first developed by Searcy and Fenn[125] shown in Figure 11. The cluster ions pass through a skimmer, and are mass selected by a magnetic mass filter before being decelerated and trapped in an octopole ion guide. After 0.5 ms the ions are irradiated with IR light before being released 1 ms later with fragment ions transmitted by

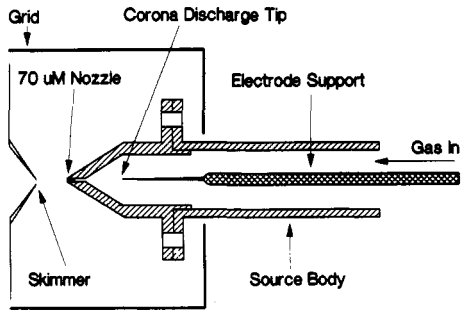

Figure 11. Corona discharge supersonic source of a type first developed by Searcy and Fenn (Ref 125) and as used by Okamura, Yeh, Lee, and co-workers in their investigations of protonated hydrogen, water, and ammonia clusters. (Reprinted from ref 151. Copyright 1991 American Chemical Society.)

a quadrupole mass filter and detected with a Daly scintillation detector.[126] The apparatus used by Bae was similar except that electron impact was used to produce the hydrogen cluster ions in the early part of the supersonic expansion.[124]

While the H_2 ligand stretch in the 4000-cm^{-1} region was observed in all the H_3^+–$(H_2)_n$ clusters with $1 < n < 6$, the perturbed H_3^+ core symmetric stretching vibration was only apparent in the H_5^+ cluster (band maximum at 3532 cm^{-1}). There is some spectral evidence that the first three ligand hydrogen molecules do indeed occupy equivalent apical sites with further ligands positioned farther from the H_3^+ core as suggested by calculations. While the band associated with the H_2 stretch increases in frequency as one goes from H_5^+ (3910 cm^{-1}) to H_7^+ (3980 cm^{-1}) to H_9^+ (4020 cm^{-1}) addition of further H_2 ligands does not result in a substantial change in the spectrum, with band centers for H_9^+ appearing at 4028 cm^{-1}, for H_{11}^+ at 4035 cm^{-1}, and for H_{13}^+ at 4048 cm^{-1}. On this basis it is suggested that the H_9^+ structure shown in Figure 9 constitutes the core of larger clusters. H_2 units add to the core are not sufficiently perturbed to have appreciable IR oscillator strength, and in turn they do not greatly affect the vibrational frequencies of the H_2 molecules closer to the core. Four broad bands have also been observed in the vibrational overtone region (5400–1000 cm^{-1}); however, the assignments appear uncertain at present.[124]

The solution of the rovibrational problem for H_5^+ can be seen as a central problem not only for cluster ion spectroscopy but also for the vibrational dynamics of five-atom systems. As noted by Yamaguchi et al.,[120] points on the H_5^+ potential hypersurface have been calculated with greater reliability than for any other five-atom system, rendering it attractive to those who wish to ascertain from first principles the rovibrational energy levels of a nonrigid five-atom system. Rotational structure has not been observed in any of the observed vibrational bands even though the predicted rotational spacing for H_5^+ is 6–7 cm^{-1}.[122,123] Theoretical determinations of the homogeneous widths of quasibound levels lying above the dissociation threshold may help decide whether the lack of structure in the spectrum between 3400 and 4200 cm^{-1} is due to lifetime broadening.

G. Ar–H_3^+

Related to the H_{2n+1} series of clusters are those where one of the ligand H_2 molecules is replaced by a rare gas atom, leading in the first instance to species of the type RG–H_3^+ (RG = He, Ne, Ar). While mass spectroscopic and ion-neutral reactivity studies[127] have been made for Ar–H_3^+, it is from the remarkable microwave absorption work on Ar–H_3^+ by Bogey et al. that the most detailed structural information on an ionic complex has come.[128,129] These studies show that the molecule has a planar C_{2v} structure with Ar adjacent to the vertex of an equilateral triangular H_3^+ (side 0.876 Å) with an Ar···H_3^+ centroid distance of 2.384 Å. Estimates for the Ar···H_3^+ bond stretching frequency and binding energy of 352 and 2300 cm^{-1}, respectively, were obtained from the centrifugal distortion constant. The latter value assumes a 12–4 Lennard-Jones potential, although if an 8–4 form of the potential is chosen instead, a binding energy of 3400 cm^{-1} is determined, which compares slightly more favorably with the calculated value of 2900 cm^{-1}.[130] It appears from the experimentally observed tunneling splittings and ab initio calculations, that the barrier for the planar internal rotation of the H_3^+ lies between 1000 and 2000 cm^{-1}.

Experimental and theoretical explorations of the properties of other RG···H_3^+ complexes have also been made. Calculations of the structure and binding energies for He–H_3^+[131] point to a C_{2v} geometry, a binding energy of 1.05 kcal/mol and a distance between the He atom and the H_3^+ center of mass of 2.95 Å. $(He)_n$–H_3^+ ($n \leq 13$) clusters have been synthesized by accretion of He atoms onto H_3^+ seed ions injected into a cooled He filled drift tube[132] although structures and binding energies for these species remain to be established.

H. Solvated Hydronium Ions

Protonated water clusters $H_3O^+(H_2O)_n$ are of particular significance because of their close relationship to the water-solvated proton and because of their abundance in the D region of the ionosphere.[133] The core hydronium ion (H_3O^+) has been characterized using high-resolution velocity modulation IR absorption in an electric discharge.[134–137] Infrared absorption studies of the protonated water cluster were initiated by Schwarz who employed a pulsed radiolysis cell in combination with a globar radiation source and monochromator to record absorptions between 2000 and 4000 cm^{-1} in $H_3O^+(H_2O)_n$ (n = 3–5) at 40-cm^{-1} resolution.[138] His method involved measuring the time-dependent absorption after cluster ion formation was initiated by the radiolysis beam and using clustering enthalpies[139] to deconvolute the measured spectra and so yield spectra of specific cluster sizes.

The earlier work has been extended by employing the technique of mass-selected cluster ion photodissociation.[140] Due to the large binding energies of the protonated water clusters, one 3000–4000-cm^{-1} IR photon is insufficient to cause cluster fission and it was necessary to employ an IR multiphoton excitation scheme to probe and fragment the clusters. Tunable light from an F-center laser is first used to excite clusters to bound levels between 3550 and 3800 cm^{-1}. Absorption of further photons from a CW CO_2 laser then takes the clusters into a vibrational quasicontinuum from where dissociation is energetically possible. Assignment of $H_3O^+(H_2O)_n$ spectral features have relied on the calculations of cluster structures, vibrational frequencies, and transition intensities by Remington and

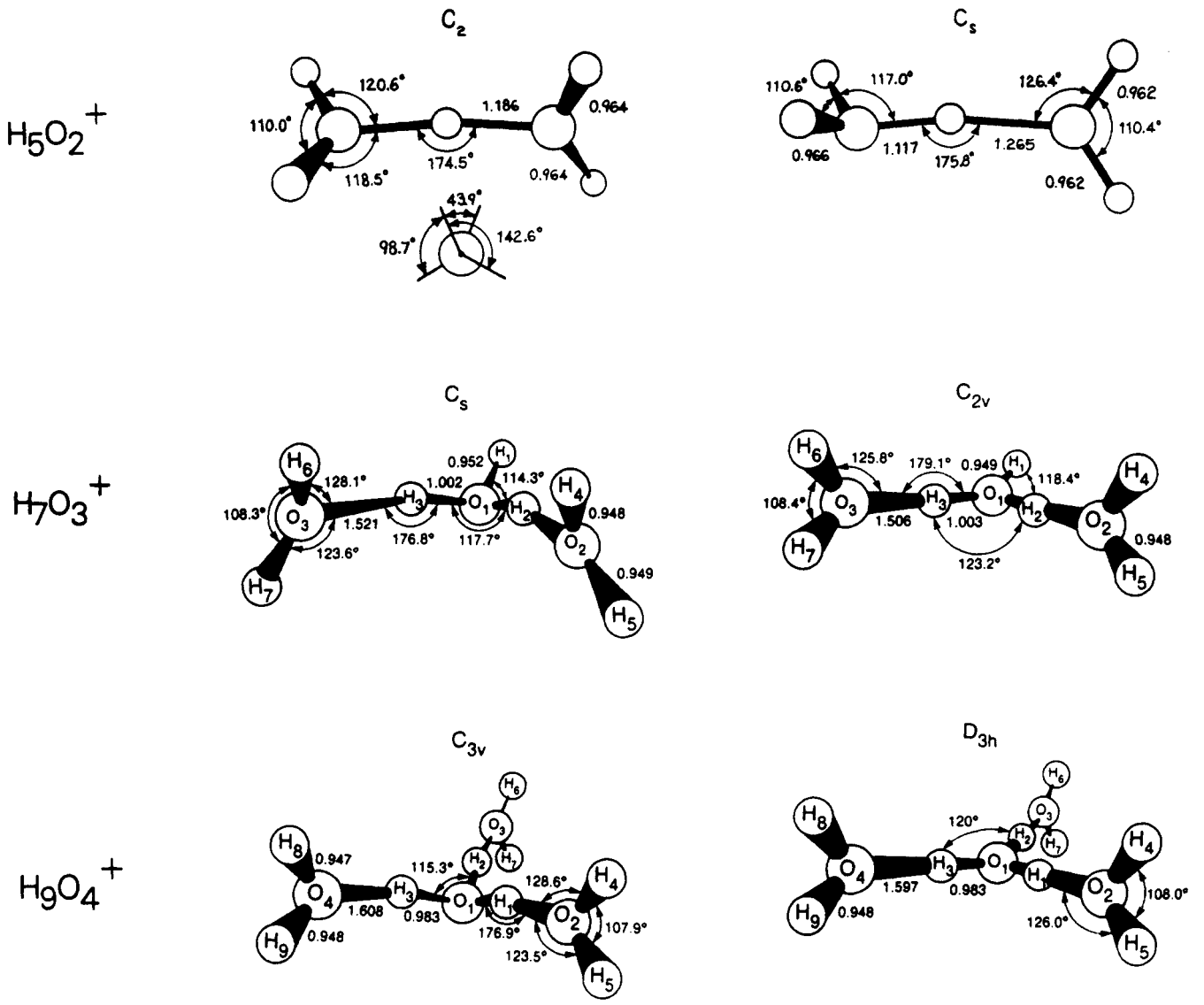

Figure 12. Lowest energy calculated structures for $H_5O_2^+$, $H_7O_3^+$, and $H_9O_4^+$ complexes. (Reprinted from ref 140. Copyright 1989 American Institute of Physics.)

Schaeffer. Predicted structures for the first few members of the series are shown in Figure 12.

Water has strongly allowed infrared transitions so that in contrast to the protonated hydrogen clusters, IR absorption by the ligands does not depend on perturbation by the cluster core. As the cluster becomes larger, the bands corresponding to H_2O symmetric and antisymmetric stretches increase in frequency, possibly due to the diminishing effect of the ion core on the solvent ligands. As shown in Figure 13 rotational structure was partially resolved for the 3684.4-cm^{-1} band of $H_5O_2^+$. The sharp peaks are assigned as a Q-branch progression with the observed spacing of 11.6 cm^{-1} consistent with the $2(A - B) = 11.65$ cm^{-1} spacing predicted for a perpendicular transition in the calculated C_2 structure shown in Figure 12.

Infrared resonant dissociation spectra have also been obtained for the hydronium ion solvated by both H_2 and H_2O ligands—$H_3O^+(H_2O)_m(H_2)_n$.[141,142] The fact that the proton affinity of H_2O is ~66 kcal/mol higher than that of H_2[143] means that these species can be approximately considered as a hydronium ion solvated by neutral H_2O and H_2 ligands.

The first member of the $H_3O^+(H_2)_n$ series—$H_3O^+(H_2)_1$ is of special interest as it represents the transition

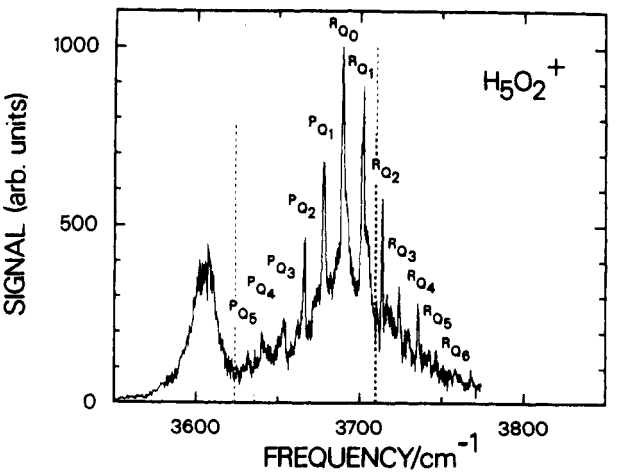

Figure 13. The infrared spectrum of $H_5O_2^+$ obtained using two-color IRMPD technique. The dashed lines correspond to calculated frequencies and intensities for the C_2 symmetry structure shown in Figure 12. (Reprinted from ref 140. Copyright 1989 American Institute of Physics.)

state for the fundamental protonation reaction: $H_3^+ + H_2O \rightarrow H_2 + H_3O^+$. Here the structure is predicted on the basis of calculations to be a hydrogen bonded one

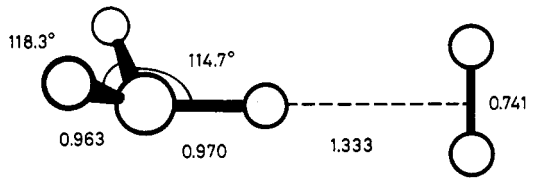

Figure 14. Geometry of $H_3O^+(H_2)$ predicted by ab initio calculations of Remington and Schaefer. Linear dimensions are in angstroms. (Reprinted from ref 142. Copyright 1990 American Chemical Society.)

as illustrated in Figure 14.[142] The infrared spectrum of $H_3O^+(H_2)_1$ exhibits bands due OH and H_2 stretches, several of which display rotational structure. The spacings in these bands accord with the calculated structure shown in Figure 14. Spectra of the larger $H_3O^+(H_2)_n$ clusters are also consistent with geometries where the H_2 ligands are hydrogen bonded to the central H_3O^+ core. From the fragmentation patterns binding energies of the H_2 ligands are estimated to be between 3.1 and 3.8 kcal/mol.[142] For clusters that include both H_2 and H_2O ligands it appears that the H_2O units preferentially occupy the sites close to the core in much the same manner as for the $H_3O^+(H_2O)_n$ structures shown in Figure 12, with the H_2 ligands left to bond either to unoccupied central sites or to the H_2O ligands.[142]

The technique of attaching a weakly interacting entity or "messenger" to an ionic cluster in the hope that excitation of vibrations localized to the ionic core will lead to mass spectroscopically detectable vibrational predissociation occurring at the frequencies of the unperturbed core ion transitions, has been employed on several occasions by the Berkeley group.[140-142] Studies show that a Ne atom perturbs the energies and transition moments of the $H_3O^+(H_2O)_n$ clusters much less than does H_2.[140] At first approximation one would expect that the degree of interaction between a protonated cluster and a ligand would depend on the ligand's proton affinity, so that Ne with a proton affinity of ~48 kcal/mol should bind less disruptively than H_2 which has a proton affinity of 101 kcal/mol.

I. Protonated Ammonia Clusters

Much of the experimental and theoretical work on the protonated ammonia clusters parallels that on the protonated water clusters. Initially high-pressure mass spectrometry measurements of Kebarle[144,145] yielded thermochemical data, while the later low-resolution absorption spectra of Schwarz pointed to the coarse features of the clusters' spectra.[146] The high-resolution infrared spectroscopy of the central NH_4^+ core (ν_3 band) has been investigated by Crofton and Oka[147,148] and Schafer and Saykally.[149] More recently, the impressive higher resolution dissociation spectra of mass selected clusters obtained by Price, Crofton, and Lee[150,151] have illuminated aspects of the structures determined in the calculations of Remington and Schaeffer.

As in the case of the analogous water species, the larger protonated ammonia clusters appear to consist of a central NH_4^+ core surrounded by solvent ammonia molecules hydrogen bonded to the core. Due to the large number of infrared-active vibrations in both the ion core and in the surrounding NH_3 ligands, the IR predissociation spectra tend to become a little confusing for these clusters. Spectral assignments have relied on

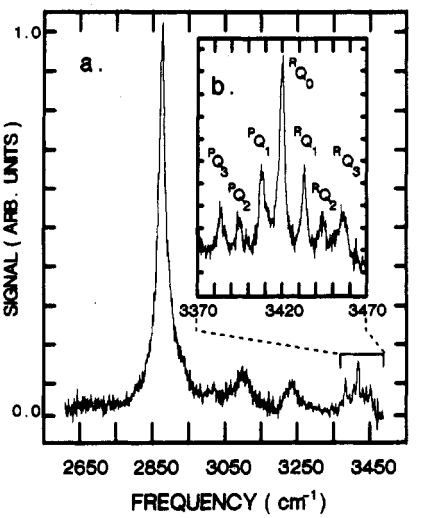

Figure 15. Infrared vibrational predissociation spectrum of $(NH_4)^+(NH_3)_4$ illustrating structure that is a consequence of internal rotation of the NH_3 solvents about their C_3 axes. Signal is product $(NH_4)^+(NH_3)_3$ counts: (a) medium resolution spectrum and (b) finer detail of the region around 3420 cm^{-1}. (Reprinted from ref 150. Copyright 1989 American Institute of Physics.)

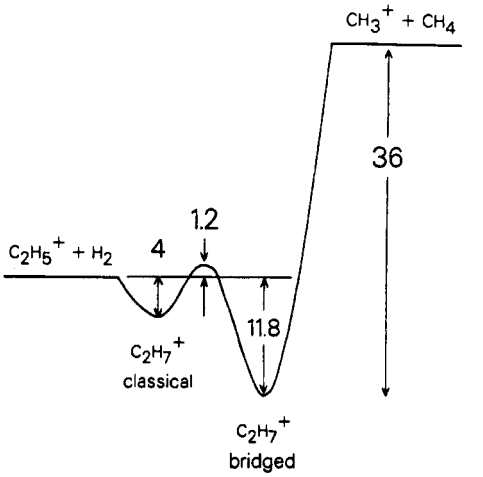

Figure 16. Energy diagram based on the thermochemical studies of ref 153 of classical and bridged structures of $C_2H_7^+$. Energies are in kcal/mol. (Reprinted from ref 152. Copyright 1989 American Chemical Society.)

arguments based on symmetry and the shifting positions of bands as more ligands are added.[150,151] Infrared-active vibrations attributable to the NH_4^+ core include the ν_3 (antisymmetric stretch), ν_1 (symmetric stretch), and $2\nu_4$ (degenerate bend). The strongest bands arising from the solvent NH_3 molecules are the ν_3 (doubly degenerate asymmetric stretch) and $2\nu_4$ (bending mode) bands.

In the smaller $(NH_4)^+(NH_3)_n$ clusters ($n < 8$), bands involving the ν_3 mode near 3420 cm^{-1} have structure that is a consequence of internal rotation of the NH_3 solvents about their C_3 axes (Figure 15). The band displays well resolved subbands separated by 12.5 cm^{-1}, roughly twice the rotational constant of ammonia about its C_3 axis.[150,151]

J. $C_2H_7^+$

The infrared dissociation spectrum of the protonated ethane cluster $C_2H_7^+$ has been important because of its bearing on the dispute between classical and bridged forms of the carbonium ions.[152] (Figure 16 shows the

energetics of classical and bridged structures derived from the thermochemical studies of Hiraoka and Kebarle.[153] The IR spectra display two sets of bands that exhibit different behavior according to the gas mixture and nozzle expansion conditions, and whether the output of a CO_2 laser is used along with the tunable IR beam. One set of bands, assigned as due to the classical structure, is most apparent when the fraction of C_2H_6 compared to H_2 is tiny and does not require additional photons from the CO_2 laser, while the other set, due to the more stable bridged structure, requires the CO_2 laser beam and persists with higher proportions of C_2H_6 in the expansion.

IV. Metal Cation–Ligand Complexes

Group I and transition metal cations bound to one or more substituent ligands have been the object of studies of four groups in the past 4 years. Three of the groups use electronic transitions to obtain spectroscopic constants and information on the bonding in these complexes characterized by charge–dipole, or charge-induced dipole interactions. The other group infers such data from the infrared vibrational transitions. In all cases the essence of the experiments is mass selection of the complex of interest, followed by laser photon absorption in the IR or visible, and detection of a fragment ion (usually the bare atomic ion) produced as a result of vibrational or electronic predissociation. In the IR experiments the discrete lines of a CO_2 laser are utilized, and for the electronic excitation studies continuously tunable, pulsed dye lasers. Two of the groups generate metal ion complexes by laser vaporization of the appropriate metal (Mg, V, Cr, CO) within a pulsed supersonic expansion of the ligand (CO_2, Ar, Kr, H_2O, N_2) in excess of helium, and the other two groups generate them by thermoemission using a filament coated with the metal (Sr, Na, Cs), again within a supersonic free jet which includes the ligand (CH_3OH, NH_3, H_2O).

In the studies utilizing electronic transitions to probe the atomic ion complexes, one induces a perturbed electronic transition of the bare metal ion whose location is well known. For example, Mg^+ has a strongly allowed ^2P–^2S transition (analogous to the D line of sodium) near 280 nm. The effect of adding a ligand to the metal ion core is illustrated schematically in Figure 17 for the case of Mg^+CO_2.[154] Two electronic transitions are observed in a similar wavelength region to the ^2P–^2S one of the metal. As can be seen in Figure 18, the lower energy of these is well structured and has $^2\Pi$–$^2\Sigma$ symmetry for a linear molecule (cf. correlation in Figure 17).[155,156] In this case only the Mg^+ product ion is detected. The vibrational structure of the band is assigned to a progression (v = 0–5) in the $Mg^+\cdots CO_2$ stretching mode ($\sim$380 cm^{-1}) in the excited electronic state. The doubling of the lines is associated with spin–orbit splitting (92 cm^{-1}). By means of a Birge–Sponer extrapolation the dissociation energy for the excited state is inferred (D_o' = 11 194 cm^{-1}), and from this, using the Mg^+ term values, the binding energy for the ground state is deduced (D_o'' = 5150 cm^{-1}). The observed spin–orbit splitting and a good agreement between the inferred vibrational constants, excitation energy, and dissociation energies,[155,156] with theoretical calculations[157] lead to the conclusion that the complex is linear.

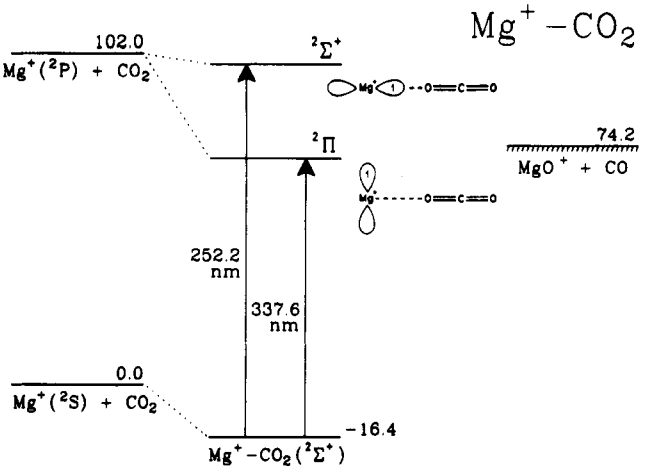

Figure 17. Energy level diagram for the Mg^+/CO_2 system. The center levels are the calculated molecular orbital energies. The energy of MgO^+ + CO is an upper limit derived from a corresponding upper limit obtained for the dissociation energy of MgO^+. (Reprinted from ref 154. Copyright 1992 American Chemical Society.)

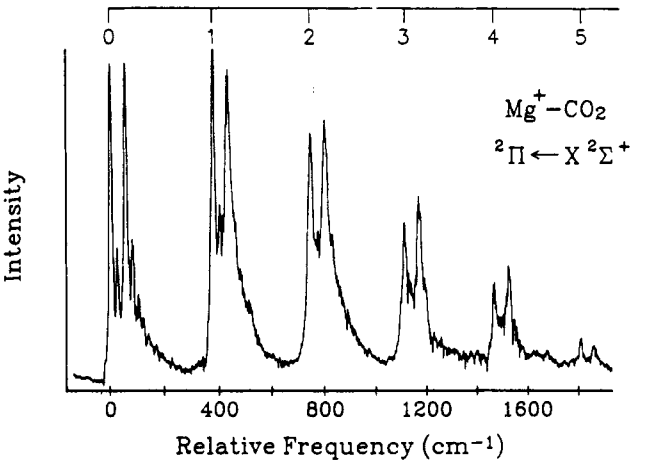

Figure 18. The photodissociation spectrum of the complex Mg^+–CO_2. The spectrum was obtained by monitoring the intensity of the Mg^+ fragment ion from the mass-selected parent while the excitation laser was scanned. The origin of the electronic spectrum is at 29 625 cm^{-1}. (Reprinted from ref 154. Copyright 1992 American Chemical Society.)

For the higher $^2\Sigma \leftarrow {}^2\Sigma$ transition, MgO^+ product ions are detected in addition to Mg^+ ions. Because MgO^+ is energetically accessible from both the excited electronic states ($^2\Sigma$,$^2\Pi$) it is argued that the preferential formation is an aligment effect.[154] In case of the $^2\Sigma$ state, the metal insertion reaction is suggested to be more efficient because of the on-axis p-AO of the metal donating to the antibonding $2\pi_u$ MO of CO_2, whereas for the $^2\Pi$ excited state, the corresponding metal p-AO is perpendicular to the interatomic axis.

Most recently the photodissociation spectrum of Mg^+H_2O has been observed in the 270–360-nm region.[158,156] Although the transition intensity is lower than with CO_2 as ligand, vibrational and to some extent rotational structure are resolved. On the basis of simple symmetry arguments, one expects three near-lying electronic states, resulting from the different orientations of the excited metal p-orbital with respect to the water molecule. In the spectrum, two electronic band systems are identified and vibrationally analyzed. For the lowest excited electronic state, one observes rich vibrational structure. By means of a vibrational

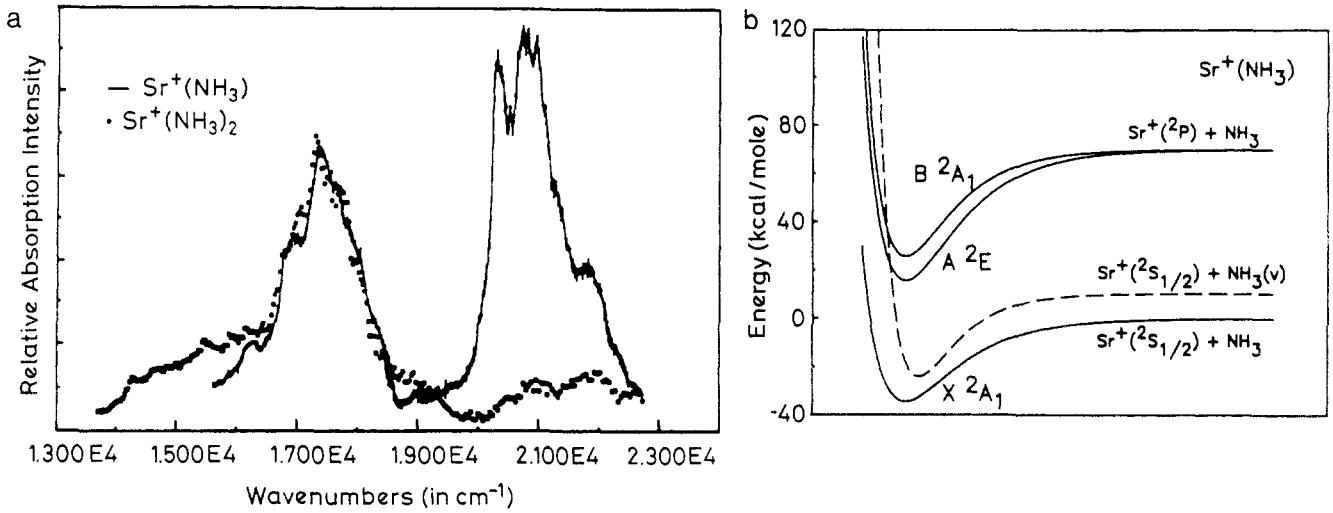

Figure 19. (a) Total photodissociation cross sections for $Sr^+(NH_3)_{1,2}$. The data are normalized to the maxima in the low-energy peaks of the absorption cross sections. Data are plotted as a function of photon energy (cm^{-1}) and wavelength. (b) Schematic potential energy curves of the $Sr^+(NH_3)_2$ systems. The dissociation may occur through an electronic predissociation mechanism, i.e., through an initially bound transition followed by a crossing to repulsive walls of a family of curves correlating with ground-state Sr^+ and vibrationally–rotationally excited NH_3 products. (Part a: Reprinted from ref 163. Copyright 1991 American Institute of Physics. Part b: Reprinted from ref 162. Copyright 1989 American Chemical Society.)

analysis, and comparison with the spectrum of Mg^+-D_2O,[156] it is possible to confirm the origin of the transition (28 396 ± 10 cm^{-1}) and identify all six fundamental modes. The vibrational assignments, and vibronic selection rules are consistent with the symmetry properties of a $^2B_2 \leftarrow {}^2A_1$ transition of an ionic complex with C_{2v} structure. A Birge–Sponer extrapolation of the extended progression in the $Mg^+\cdots H_2O$ stretching mode (ω_e = 518 cm^{-1}) yields the excited state dissociation energy (~16 000 cm^{-1}), and then the ground-state value (~8500 cm^{-1}) from the known Mg^+ energetics. There is good agreement of the experimentally inferred vibrational frequencies and dissociation energies and those calculated for an optimized C_{2v} structure.[159] The C_{2v} structure is supported by simulation of the partially resolved rotational contours (at a rotational temperature ≈ 10 K), which reproduce the experimental data for a Mg···O distance of 2.026 Å in the ground state. 1.969 Å in the excited one, and a H–O–H bond angle of 109°. The calculations and the spectral observations indicate that the system is characterized by weak electrostatic bonding, where although the ligand is polarized by the metal centered positive charge, its character is not greatly perturbed (e.g. similarity of the vibrational frequency of free and complexed H_2O). The second electronic transition with origin at 30 267 cm^{-1} is of $^2B_1 \leftarrow {}^2A_1$ symmetry and the analysis yields the frequencies of four fundamental vibrations in the excited state.

In another study,[160] similar photodissociation spectra have been reported for Mg^+H_2O and $Mg^+(H_2O)_2$, though no vibrational structure was resolved. Assignments of the electronic transitions were as discussed above, with a C_{2v} symmetry structure deduced for Mg^+H_2O. For $Mg^+(H_2O)_2$, a bent C_2 symmetry geometry with a staggered arrangement of the H_2O moieties was inferred.

In the photodissociation studies of Sr^+ solvated by ammonia or water molecules, the information on the bonding and interactions is again inferred from the electronic spectra.[161-163] The observed transitions are significantly shifted with respect to those in the free atom. The spectra for Sr^+L, L = NH_3, H_2O were recorded by monitoring the intensity of the Sr^+ ion produced by an electronic predissociation process. For the complexes with more than one ligand Sr^+L_n, both Sr^+ and Sr^+L_{n-1} fragment ions were monitored. By these means the mass-selected complexes $Sr^+(NH_3)_n$ (n = 1–4) and $Sr^+(H_2O)_n$ (n = 1, 2) have been studied. The dissociation energy in the excited state of Sr^+H_2O (D_0' ≈ 1.94 eV) is estimated from the onset of the photodissociation spectrum. Barely resolvable vibrational structure is most probably due to extensive sequence bands,[161] implying that the cluster ions are vibrationally quite hot.

As an example, the measured spectra for $Sr^+(NH_3)_n$ (n = 1, 2) are shown in Figure 19, where also the pertinent potential energy curves and dissociation limits are schematically drawn.[162] The 560-nm band is based on a ^2S–^2P transition of Sr^+ (^2E–$^2A_1$ in C_{3v} molecular symmetry). The 480-nm band is assigned to a $^2A_1$–$^2A_1$ transition, again localized mainly on the strontium ion. The spectra of $Sr^+(NH_3)_n$ (n = 3, 4) show a new absorption feature to lower wavelengths (680 nm for n = 3; 900 nm for n = 4).[162] These are ascribed to an intramolecular electron-transfer transition associated with $Sr^{2+}(NH_3)_{n-m}(NH_3)_m^-$ excited-state structure.

The photodissociation spectra of $Sr^+(H_2O)_n$ (n = 1, 2) have also been recorded (Figure 20).[162] The principal difference between the n = 1 complex of H_2O (C_{2v} symmetry) and that of NH_3 (C_{3v}) is the appearance of three bands rather than two as consequence of the removal of the degeneracy of the ^2E excited electronic state. The similarity of the spectra for the complexes with one or two water molecules attached implies that the transition is essentially a localized atomic transition. The main drawback of these measurements appears to be the apparent high internal excitation of the complex ions.

The spectra of the Sr^+L_n (L = NH_3, H_2O) complexes were rationalized with a simple molecular orbital analysis, assuming atom, and ligand basis orbitals.[163] The electrostatic interactions are included via the off-diagonal elements in a Hückel-type approach. This accounts for the smaller red shift (relative to the free atom transition), and reduced width, of the bands for the H_2O complexes compared to their NH_3 counter-

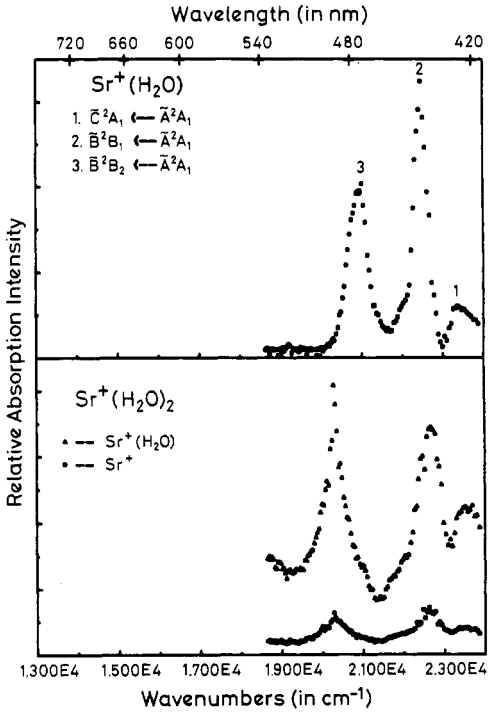

Figure 20. Photodissociation spectrum for $Sr^+(H_2O)_1$, showing Sr^+ counts as a function of photon energy and wavelength. Band assignments are discussed in the text. The lower panel shows the photodissociation spectra for $Sr^+(H_2O)_2$, showing signals for $Sr^+(H_2O)$ and Sr^+. (Reprinted from ref 163. Copyright 1991 American Institute of Physics.)

parts: a consequence of the 2.4 eV larger ionization potential of H_2O and the resulting reduced interactions with the Sr^+-based orbitals.

The studies of Lisy and co-workers are focused on similar systems, $Cs^+(CH_3OH)_n$ (n = 4–16)[164,165] and $Na^+(NH_3)_m$ (m = 6–12),[166] although the experiments are carried out in the infrared. A multiline CO_2 laser is used to excite either the ν_4 (C–O stretch) of the CH_3OH ligand or the ν_2 (N–H bend) of NH_3. The vibrationally excited mass-selected cluster ion undergoes vibrational predissociation leading to a decrease in intensity in the parent ion signal. Spectra are obtained by recording the depletion as function of the IR laser wavelength. Spectra of the $Cs^+(CH_3OH)_n$ (n = 4–16) complexes show a broad maximum centered around 1031 cm^{-1}, whereas CH_3OH itself absorbs at 1034 cm^{-1} in the gas phase.[164] For n = 4–10 there is only a single peak; however, for n = 11–16, a second broad peak appears at ~1040 cm^{-1} (Figure 21).[165] The interpretation of this is that the first solvent shell comprises 10 methanol molecules, after which the second shell starts to be filled. With n = 19–25, another feature attributable to the development of the third solvation shell appears in the spectrum (Figure 21 lower).

The interpretation is supported by Monte Carlo simulations using model pairwise interaction potentials.[165] These suggest that in the first shell the O atoms are nearest to Cs^+ and emphasize the importance of hydrogen bonding to cluster structure. Close to 90% of the solvation enthalpy is accounted for by the first shell. The second shell requires 6–8 CH_3OH ligands however the methanol molecules start to occupy the third shell before the second one is completely filled.

A corresponding study on $Na^+(NH_3)_n$ (m = 6–12) has been performed.[166] Vibrational predissociation spectra are observed only for $m \geq 6$ and the two main spectral

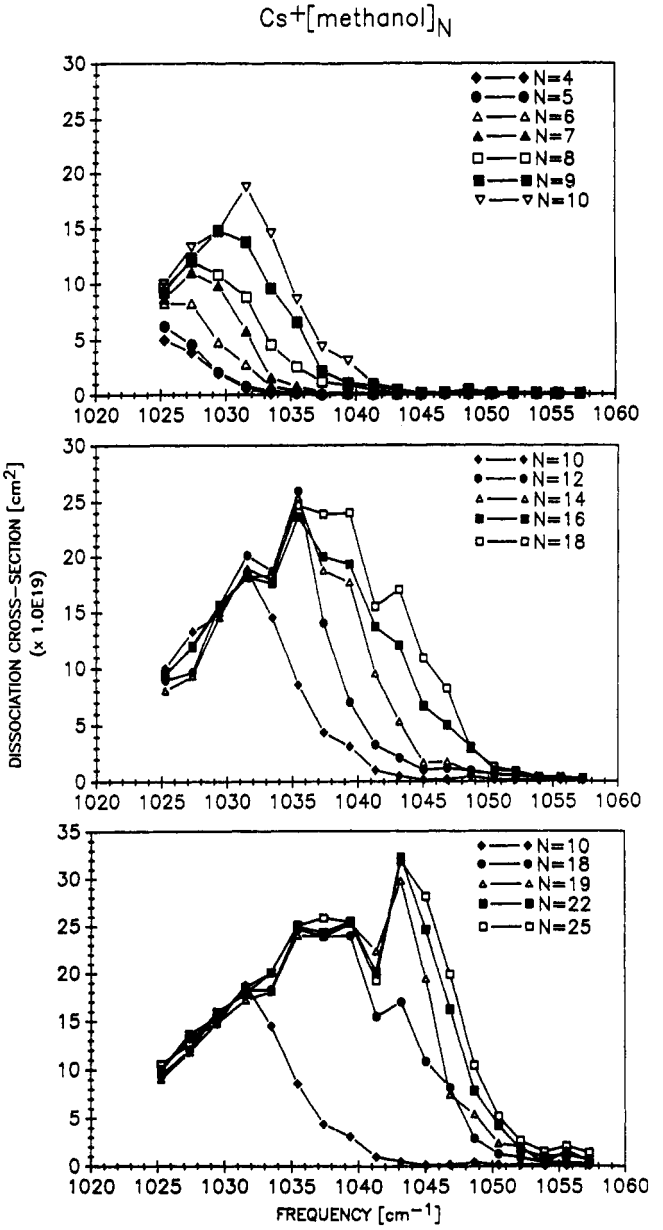

Figure 21. Photodissociation spectra of $Cs(CH_3OH)_n^+$. (Reprinted from ref 165. Copyright 1990 American Institute of Physics.)

features are interpreted as (1) a peak at ~1085 cm^{-1} for m = 6–9 is characteristic of an isolated ammonia molecule coordinated to other ammonia molecules in the first solvent shell; (2) for $m > 9$ two to three further absorption peaks appear in the 1045–1080-cm^{-1} region that have previously been associated with larger pure ammonia clusters and liquid ammonia. These observations are taken as an indication of the onset of bulklike behavior.

The nature of the binding in solvated metal ions of V^+L with L = Ar, Kr,[167] H_2O,[168] Cr^+L with L = Ar, N_2,[169] Ni^+Ar,[170] and Co^+L with L = Ar, Kr[171] has been investigated by electronic-predissociation spectroscopy with a tunable, pulsed dye laser. For this purpose, the metal ions are produced by laser vaporization of a metal rod within a supersonic pulse of a carrier gas, the latter consisting of a mixture of the ligand in helium.

Most of the spectra show resolved vibrational structure, as illustrated in Figure 22 for Co^+Ar.[171] Three band systems are identified, A ← X, B ← X, C ← X, with the extensive vibrational progressions of up to v'

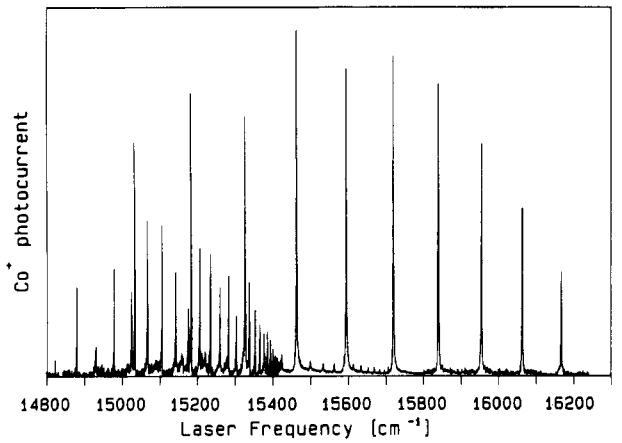

Figure 22. A portion of the $CoAr^+$ resonant photodissociation spectrum. The smaller dissociation at the low- and high-frequency ends of the plot represent a drop-off in the dissociation laser output intensity and not a systematic change in the peak dissociation cross section. Three upper-state vibrational progressions corresponding to three different electronic states are evident in the figure. (Reprinted from ref 172. Copyright 1990 Elsevier.)

Table III. Experimentally Determined Ground (D_e'') and Excited State Binding Energies (D_e') Binding Energies of Transition Metal–Rare Gas Diatomic Cations (from Ref 172. Copyright 1990 Elsevier.)[a]

ion	configuration	D_e'' (eV)	D_e' (eV)
VAr^+	$3d^4$	0.381	
VAr^+	$3d^34s$		0.175
$CrAr^+$	$3d^5$	0.27	
$CoAr^+$	$3d^8$	0.524	
$CoAr^+$ (A state)			0.331
$CoAr^+$ (B state)	$3d^74s$		0.254
$CoAr^+$ (C state)	$3d^8$		0.36
VKr^+	$3d^4$	0.485	
VKr^+	$3d^34s$		0.263
$CoKr^+$	$3d^8$	0.682	
$CoKr^+$ (A state)			0.455
$CoKr^+$ (B state)	$3d^74s$		0.354
$CoKr^+$ (C state)	$3d^8$		0.494
$LiAr^+$	$1s^2$	0.550[b]	
		0.303[c]	
		0.276[d]	
		0.318[e]	
$NaAr^+$	$2s^22p^6$	0.211[b]	
		0.119[f]	
KAr^+	$3s^23p^6$	0.119[b]	
		0.064[f]	
		0.085[g]	
		0.12[h]	
		0.14[i]	

[a] Metal ion atomic configuration in separated atom limit. [b] Reference 173. [c] Reference 174. [d] Reference 175. [e] Reference 176. [f] Reference 177. [g] Reference 178. [h] Reference 179. [i] Reference 180.

= 35, 41, and 46, respectively, allowing the determination of ω_e and $\omega_e x_e$ vibrational constants. The dissociation energies of the metal ion complexes in their excited states were evaluated from the vibrational data by fitting the spacings of the higher vibrational levels with those expected to arise from the long-range $1/r^4$ charge ion-induced dipole force. A knowledge of the relevant dissociation limits allows the ground state values to be obtained. Values for the studied metal ion complexes are given in Table III.[172] The variation apparent for the D_o'' values listed in the Table III is rationalized by noting that for transition metal cations with more than half-filled d subshells the 3d orbitals

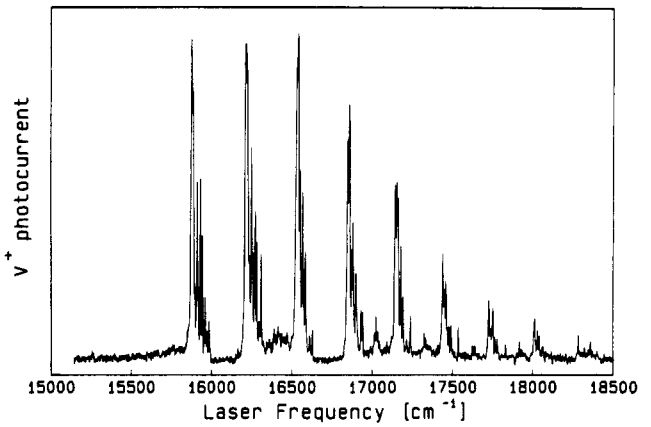

Figure 23. Resonant photodissociation of $V(OH_2)^+ \rightarrow V^+ + H_2O$. Noticeable is a vibrational progression with frequency of ca. 350 cm^{-1} and the complex substructure associated with each band. This vibrational progression is assigned to the $V–H_2O$ stretch via isotope shifts, firmly establishing this ion as electrostatically bound and not an inserted (H–V–OH) structure. (Reprinted from ref 168. Copyright 1990 American Institute of Physics.)

contract with increasing nuclear charge allowing a closer approach of the rare gas atom and an decrease in the ion-induced dipole interaction energy.

The interactions in such metal ion complexes were modeled with a two adjustable-parameter potentials:[172] $U(r) = b \exp(-r/\rho) - q^2\alpha/(2r^4)$ where α is the polarizability of the rare gas atom. The parameters b and ρ were varied so that calculated D_o' and ω_e' values agreed with the experimental values. For the ground state, ω_e'' was not available directly but was determined by varying the one adjustable parameter of an 8–4 Lennard-Jones potential to yield the experimentally determined D_o''. Experimentally it is observed that $CoAr_6^+$ [181] and VAr_4^+ [167] appear to have especially stable structures. Using the empirically determined potentials for the metal ion–argon interactions and by including the Lennard-Jones (12,6) potential for the two body argon–argon ones, the geometry of the complexes was optimized. These simulations suggest that for VAr_{14}^+ the bulk limit has almost been reached and that all VAr_n^+ ($n \geq 4$) clusters have a tetrahedral core with four argon atoms constituting the first solvation shell.

One transition metal ion complexed with a molecular ligand has also been investigated—$V^+(H_2O)$. The measured electronic spectrum is reproduced in Figure 23.[168] By studying the ^{18}O and ^2H isotopically substituted derivatives, it has been shown that the spectrum is due to an electrostatically bound $V^+\cdots H_2O$ structure. The analysis leads to $\omega_e'' = 420 \pm 75$ cm^{-1}, $\omega_e' = 339 \pm 5$ cm^{-1}, and $D_e' \leq 1.97$ eV.

V. Negative Ion Clusters

Of the experiments carried out on anion clusters, the majority have focused their attention to the study of photofragmentation pathways [C_n^- ($4 \leq n \leq 20$); $(H_2O)_n^-$],[182,183] [$Br_2^-(CO_2)_n$ ($n \leq 24$); $I_2^-(CO_2)_n$ ($n \leq 16$)].[185,186] Only the few studies involving the photoelectron spectra of mass-selected anions leading to relatively direct conclusions on the structure of the complexes are discussed here. Anions are formed either in an electron-beam crossed-seeded pulsed supersonic

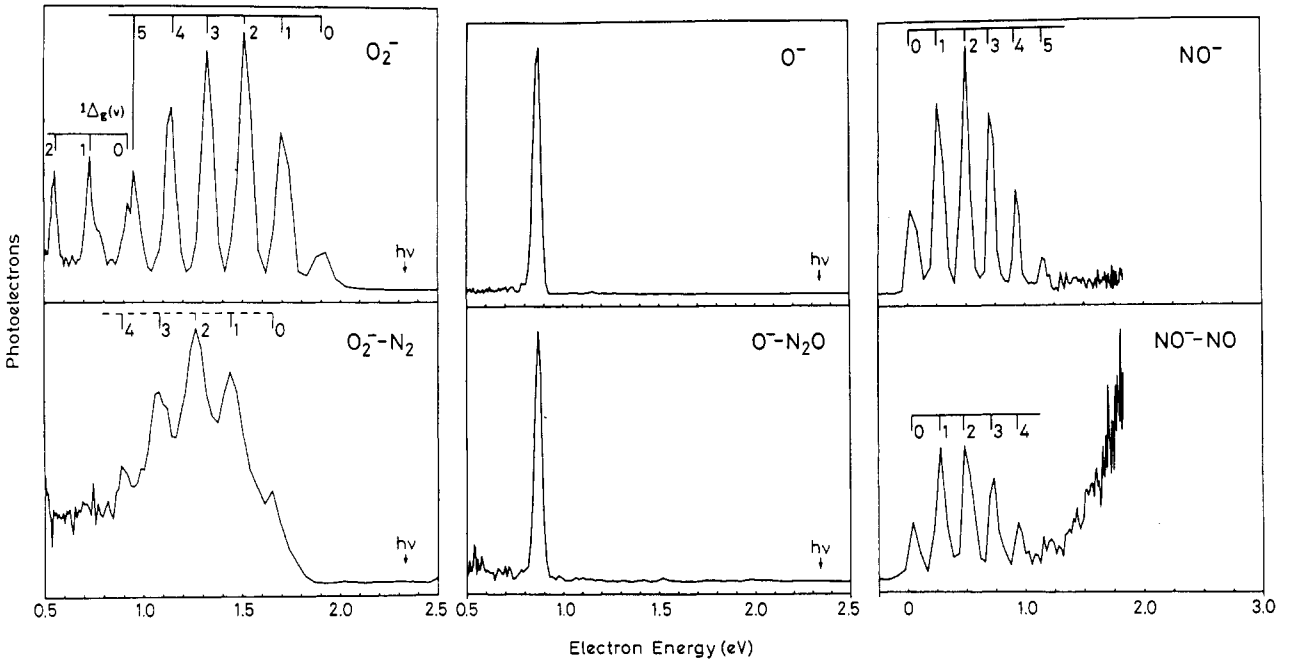

Figure 24. Photoelectron spectra taken at 532 nm of (left) O_2^- and O_2^-–N_2 (from 5% O_2 in N_2), (middle) O^- and O^-–N_2O (from neat N_2O), and (right) NO^- and NO^-–NO (from NO/Ar). (Reprinted from ref 184. Copyright 1988 American Institute of Physics.)

expansion with the anions formed by dissociative electron attachment on the neutral clusters,[187] or by continuous production in an anion source.[188] After mass selection, either by time of flight in the pulsed source, or Wien filter in the cw one, the photoelectron spectrum is measured following irradiation with a pulsed Nd: YAG (355 nm) or cw Ar^+ (488 nm) laser in the two approaches, respectively. The pulsed studies investigated the $(CO_2)_n^-$, $(O_2)_n^-$, $(CO_2)_nH_2O^-$, $I^-(CO_2)_n$, and $N_2O_2^-$ species and the cw ones $NO^-(N_2O)_n$.

The clearest example of spectroscopic evidence for different geometric structures is for the $N_2O_2^-$ anions.[184] Using three different precursors in the supersonic expansion, one obtains characteristically distinct photoelectron spectra for the mass-selected $N_2O_2^-$ anions. In one case when O_2 is seeded in N_2, the structure is inferred to be O_2^-–N_2, because apart from a small energy shift the photoelectron spectrum is very similar to that of O_2^-. This is seen in Figure 24 (left). It can also be deduced that the binding energy of the anion complex is 0.26 ● 0.03 eV. On the other hand, $N_2O_2^-$ produced with N_2O as source gas in the expansion leads to a single photoelectron peak [Figure 24 (middle)], near the electron affinity of O^-, suggesting an O^-–N_2O structure. The third spectrum of $N_2O_2^-$, synthesized this time from NO in Ar, resembles that of NO^- [electron affinity 0.02 eV, Figure 24 (right)], leading to the conclusion that the structure is that of NO^-–NO. An earlier study[188] also used photoelectron spectroscopy to surmise that the structure of $N_3O_2^-$ and $N_2O_5^-$ anions is $NO^-(N_2O)_n$ (n = 1, 2) on the basis of the similarity of the spectra with that of NO. The dissociation energy of these two anion complexes was inferred to be ~0.22 and 0.26 eV respectively.

In the case of the $(CO_2)_n^-$ and $(O_2)_n^-$ clusters, the photoelectron spectra are featureless and the structural inferences are made on the basis of the determined vertical detachment energies. Thus for $(CO_2)_n^-$ these values increase from n = 2–5 and are interpreted as changes in solvation of a dimer core ion of D_{2d} symmetry[189] on addition of each additional CO_2. At n = 6 the detachment energy decreases by ~0.8 eV but then increases again steadily for $n > 6$. This is ascribed to a change in the structure of the core ion, from the dimeric to a monomeric one at n = 6.

In one related study,[190] the photoelectron spectra of $(CO_2)_nH_2O^-$ (n = 2–8) were investigated and show a discontinuity in the vertical detachment energies between n = 3 and n = 4. This is explained in an analogous way to the carbon dioxide anion clusters: the $(CO_2)_2^-$ dimer is the core for $n \leq 3$, but for $n \geq 4$ it is the solvated monomer.

The other investigations have concerned $I^-(CO_2)_n$ (n = 1–13), complexes which are bound by electrostatic charge–quadrupole interactions.[191] After their production from 2% HI in CO_2 in an electron-beam crossed-pulsed free jet, the photoelectron spectra of the mass-selected anion complex were measured. The spectra show two main peaks, correlating with the $^2P_{3/2}$ and $^2P_{1/2}$ states of I, within which vibrational structure is discernible to different degree depending on the peak and size of the anion complex. The progressions involve the bending vibrational mode of the solvating CO_2 molecules with frequencies in the 665 ± 90-cm^{-1} range. These photoelectron spectra were in fact measured before,[192] but the vibrational structure was not resolved.

An analysis of the spectral data is taken to indicate that in I^-CO_2, which is expected to be T-shaped, the CO_2 ligand is slightly bent. A one-dimensional Franck–Condon simulation of the peak intensity distribution leads to an OCO angle of 175°. The overall peak widths, and presence or absence of vibrational structure, are interpreted as indicating that with increasing n the OCO ligands approach tend to become linear and occupy equivalent sites and that a closed solvation shell sets in with at least nine CO_2 molecules.

For the $(O_2)_n^-$ system,[182] both the photoelectron spectra and photofragmentation patterns were studied. It appears that for $n \geq 2$ the excess electron delocalizes on an O_4^- core within the cluster. The observed

photoabsorption is attributed to a charge transfer transition from the O_4^- ion core to the O_2 solvent–ligand.

VI. Conclusions

The aim of this review has been to furnish an assessment of the current status of ionic complex spectroscopic research. The reader has probably become aware of the conspicuous gaps in our present knowledge and that, despite the volume of published material, many questions remain open. Scant progress has been made in the characterization of whole classes of ionic complexes (e.g. anionic complexes) and there are few ionic complexes for which the quality of spectroscopic data matches that obtained for neutral complexes. Reliable potential energy surfaces and rovibrational energy levels have been calculated for only a handful of molecules. With such outstanding problems the following years are worth looking forward to.

Acknowledgments. The studies in Basel have been financed by the Swiss Science Foundation (no. 20-36153.92).

References

(1) Wayne, R. P. *Chemistry of Atmospheres*; Clarendon Press: Oxford, 1991.
(2) Kebarle, P. In *Ion-Molecule Reactions*; Franklin, J. L., Ed.; Plenum Press: New York, 1972.
(3) Kebarle, P. *Ann. Rev. Phys. Chem.* **1977**, *28*, 445.
(4) Castleman, A. W., Jr.; Keesee, R. G. *Chem. Rev.* **1986**, *86*, 589.
(5) Garvey, J. F.; Pfeifer, W. R.; Coolbaugh, M. T. *Acc. Chem. Res.* **1991**, *24*, 48.
(6) Müller-Dethlefs, K.; Schlag, E. W. *Ann. Rev. Phys. Chem.* **1991**, *42*, 109.
(7) Miller, S.; Tennyson, J. *J. Chem. Phys.* **1987**, *87*, 6648.
(8) Miller, S.; Tennyson, J.; Follmeg, B.; Rosmus, P.; Werner, H. *J. Chem. Phys.* **1988**, *89*, 2178.
(9) Bowers, M. T. In *Ion and Cluster Ion Spectroscopy and Structure*; Maier, J. P., Ed.; Elsevier: Amsterdam, 1989.
(10) Maas, J. G.; Asselt, N. P. F. B. v.; Nowak, P. J. C. H.; Los, J.; Peyerimhoff, S. D.; Buenker, R. *J. Chem. Phys.* **1976**, *17*, 217.
(11) Yu, N.; Wing, W. H. *Phys. Rev. Lett.* **1987**, *59*, 2055.
(12) Rosi, M.; Bauschilicher, C. W., Jr. *Chem. Phys. Lett.* **1989**, *159*, 479.
(13) Lee, L. C.; Smith, G. P. *Phys. Rev. A* **1979**, *191*, 2329.
(14) Hiraoka, K.; Mori, T. *J. Chem. Phys.* **1990**, *92*, 4408.
(15) Ng, C. Y.; Trevor, D. J.; Mahan, B. H.; Lee, Y. T. *J. Chem. Phys.* **1977**, *66*, 446.
(16) Norwood, K.; Guo, J.; Ng, C. Y. *J. Chem. Phys.* **1989**, *90*, 2995.
(17) Morioka, Y.; Ogawa, M.; Matsumoto, T.; Ito, K.; Tanaka, K.; Hayaishi, T. *J. Phys. B: At. Mol. Opt. Phys.* **1991**, *24*, 791.
(18) Norwood, K.; Luo, G.; Ng, C. Y. *J. Chem. Phys.* **1989**, *90*, 4689.
(19) Abouaf, R.; Huber, B. A.; Cosby, P. C.; Saxon, R. P.; Moseley, J. T. *J. Chem. Phys.* **1978**, *68*, 2406.
(20) Ng, C. Y.; Trevor, D. J.; Mahan, B. H.; Lee, Y. T. *J. Chem. Phys.* **1976**, *65*, 4327.
(21) Hausamann, D.; Morgner, H. *Mol. Phys.* **1985**, *54*, 1085.
(22) Tanaka, Y.; Yoshino, K.; Freeman, D. E. *J. Chem. Phys.* **1975**, *62*, 4484.
(23) Dabrowski, I.; Herzberg, G. *J. Mol. Spectrosc.* **1978**, *73*, 183.
(24) Carrington, A.; Softley, T. P. *Chem. Phys.* **1985**, *92*, 199.
(25) Dabrowski, I.; Herzberg, G.; Yoshino, K. *J. Mol. Spectrosc.* **1981**, *89*, 491.
(26) Dehmer, P. M.; Pratt, S. T. In *Photophysics and Photochemistry in the Vacuum Ultraviolet*; McGlynn, S. P., Findley, G. L., Huebner, R. H., Eds.; 1985; pp 467.
(27) Holland, F.; Huber, K. P.; Hoy, A. R.; Lipson, R. H. *J. Mol. Spectrosc.* **1991**, *145*, 164.
(28) Dehmer, P. M.; Pratt, S. T. *J. Chem. Phys.* **1982**, *77*, 4807.
(29) Huber, K. P.; Lipson, R. H. *J. Mol. Spectrosc.* **1986**, *119*, 433.
(30) Paterson, P. L. *J. Chem. Phys.* **1968**, *48*, 3625.
(31) Deluca, M. J.; Johnson, M. A. *Chem. Phys. Lett.* **1989**, *162*, 445.
(32) Bowers, M. T.; Palke, W. E.; Robins, K.; Roehl, C.; Walsh, S. *Chem. Phys. Lett.* **1991**, *180*, 235.
(33) Gotts, N. G.; Hallet, R.; Smith, J. A.; Stace, A. *J. Chem. Phys. Lett.* **1991**, *181*, 491.
(34) Chen, Z. Y.; Albertoni, C. R.; Hasegawa, M.; Kuhn, R.; Castleman, A. W., Jr. *J. Chem. Phys.* **1989**, *89*, 4019.
(35) Levinger, N. E.; Ray, D.; Murray, K. K.; Mullin, A. S.; Schultz, C. P.; Lineberger, W. C. *J. Chem. Phys.* **1988**, *91*, 71.
(36) Woodward, C. A.; Upham, J. E.; Stace, A. J.; Murrell, J. N. *J. Chem. Phys.* **1989**, *91*, 7612.
(37) Magnera, T. F.; Michl, J. *Chem. Phys. Lett.* **1992**, *192*, 99.
(38) Jarrold, M. F.; Illies, A. J.; Bowers, M. T. *J. Chem. Phys.* **1984**, *81*, 214.
(39) Linn, S. H.; Ono, Y.; Ng, C. Y. *J. Chem. Phys.* **1981**, *74*, 3342.
(40) Norwood, K.; Luo, G.; Ng, C. Y. *J. Chem. Phys.* **1989**, *91*, 849.
(41) Carnovale, F.; Peel, J. B.; Rothwell, R. G. *J. Chem. Phys.* **1988**, *88*, 642.
(42) Conway, D. C.; Janik, G. S. *J. Chem. Phys.* **1970**, *53*, 1859.
(43) Durden, D. A.; Kebarle, P.; Good, A. *J. Chem. Phys.* **1969**, *50*, 805.
(44) Norwood, K.; Guo, J.; Luo, G.; Ng, C. Y. *Chem. Phys.* **1989**, *129*, 109.
(45) Illies, A. J.; Jarrold, M. F.; Wagner-Redeker, W.; Bowers, M. T. *J. Am. Chem. Soc.* **1985**, *107*, 2842.
(46) Jarrold, M. F.; Misev, L.; Bowers, M. T. *J. Chem. Phys.* **1984**, *81*, 4369.
(47) Teng, H. W.; Conway, D. C. *J. Chem. Phys.* **1973**, *59*, 2316.
(48) Kim, H.; Bowers, M. T. *J. Chem. Phys.* **1990**, *93*, 1158.
(49) Nagata, T.; Kondow, T. *Z. Phys. D.* **1991**, *20*, 153.
(50) Sato, K.; Achiba, Y.; Kimura, K. *J. Chem. Phys.* **1984**, *80*, 57.
(51) Takahashi, M. *J. Chem. Phys.* **1992**, *96*, 2594.
(52) Norwood, K.; Ali, A.; Ng, C. Y. *J. Chem. Phys.* **1991**, *95*, 8029.
(53) Prest, H. F.; Tzeng, W.; Brom, J. M., Jr.; Ng, C. Y. *J. Am. Chem. Soc.* **1983**, *105*, 7531.
(54) Ono, Y.; Ng, C. Y. *J. Chem. Phys.* **1982**, *77*, 2947.
(55) Ono, Y.; Linn, S. H.; Tzeng, W.; Ng, C. Y. *J. Chem. Phys.* **1984**, *80*, 1482.
(56) Tzeng, W.; Ono, Y.; Linn, S. H.; Ng, C. Y. *J. Chem. Phys.* **1985**, *83*, 2813.
(57) Ohashi, K.; Nishi, N. *J. Chem. Phys.* **1991**, *95*, 4002.
(58) Ohashi, K.; Nishi, N. *J. Chem. Phys.* **1993**, *98*, 390.
(59) Snodgrass, J. T.; Dunbar, R. C.; Bowers, M. T. *J. Phys. Chem.* **1990**, *94*, 3648.
(60) Ostrander, S. C.; Sanders, L.; Weisshaar, J. C. *J. Chem. Phys.* **1985**, *84*, 529.
(61) Norwood, K.; Guo, J.; Luo, G.; Ng, C. Y. *J. Chem. Phys.* **1989**, *90*, 6026.
(62) Linn, S. H.; Ng, C. Y. *J. Chem. Phys.* **1981**, *75*, 4921.
(63) Norwood, K.; Guo, J.; Luo, G.; Ng, C. Y. *J. Chem. Phys.* **1988**, *88*, 4098.
(64) Ng, C. Y.; Tiedemann, P. W.; Mahan, B. H.; Lee, Y. T. *J. Chem. Phys.* **1977**, *66*, 3985.
(65) Fischer, I.; Strobel, A.; Staecker, J.; Niedner-Schattenburg, G.; Bondybey, V. E. *J. Chem. Phys.* **1992**, *96*, 7171.
(66) Ono, Y.; Linn, S. H.; Prest, H. F.; Gress, M. E.; Ng, C. Y. *J. Chem. Phys.* **1980**, *73*, 2523.
(67) Tzeng, W.; Yin, H.; Leung, W.; Luo, J.; Nourbakhsh, S.; Flesch, G. D.; Ng, C. Y. *J. Chem. Phys.* **1988**, *88*, 1658.
(68) Ono, Y.; Osuch, E. A.; Ng, C. Y. *J. Chem. Phys.* **1981**, *74*, 1645.
(69) Erikson, J.; Ng, C. Y. *J. Chem. Phys.* **1981**, *75*, 1650.
(70) Linn, S. H.; Brom, J. M., Jr.; Liao, C. L.; Liao, C. X.; Ng, C. Y. *Chem. Phys. Lett.* **1984**, *105*, 645.
(71) Linn, S. H.; Brom, J. M., Jr.; Tzeng, W.; Ng, C. Y. *J. Chem. Phys.* **1985**, *82*, 648.
(72) Liao, C. L.; Ng, C. Y. *J. Chem. Phys.* **1986**, *84*, 1142.
(73) Chewter, L. A.; Müller-Dethlefs, K.; Schlag, E. W. *Chem. Phys. Lett.* **1987**, *135*, 219.
(74) Kennedy, R.; Miller, T. A. *J. Chem. Phys.* **1986**, *85*, 2326.
(75) Dimauro, L. F.; Heaven, M.; Miller, T. M. *Chem. Phys. Lett.* **1984**, *104*, 526.
(76) Kung, C.; Miller, T. A. *J. Chem. Phys.* **1990**, *92*, 3297.
(77) Kung, C.; Miller, T. A.; Kennedy, R. A. *Philos. Trans. R. Soc. Ser. A* **1988**, *324*, 223.
(78) Takahashi, M.; Ozeki, H.; Kimura, K. *J. Chem. Phys.* **1992**, *96*, 6399.
(79) Zhang, X.; Smith, J. M.; Knee, J. L. *J. Chem. Phys.* **1992**, *97*, 2843.
(80) Bieske, E. J.; Rainbird, M. W.; Knight, A. E. W. *J. Chem. Phys.* **1989**, *91*, 752.
(81) Nimlos, M. R.; Young, A.; Bernstein, E. R. B.; Kelly, D. F. *J. Chem. Phys.* **1989**, *91*, 5268.
(82) Dopfer, O.; Reiser, G.; Lindner, R.; Henri, G.; Müller-Dethlefs, K. *Ber. Bunsen-Ges. Phys. Chem.* **1992**, *96*, 1259.
(83) Reiser, G.; Dopfer, O.; Lindner, R.; Henri, G.; Müller-Dethlefs, K.; Schlag, E. W.; Colson, S. D. *Chem. Phys. Lett.* **1991**, *181*, 1.
(84) Bieske, E. J.; Rainbird, M. W.; Knight, A. E. W. *J. Phys. Chem.* **1990**, *94*, 3962.
(85) Bieske, E. J.; McKay, R. I.; Bennett, F. R.; Knight, A. E. W. *J. Chem. Phys.* **1990**, *92*, 4620.
(86) McKay, R. I.; Bieske, E. J.; Atkinson, I. M.; Bennett, F. R.; Bradley, A. J.; Rainbird, M. W.; Rock, A. B.; Uichanco, A. S.; Knight, A. E. W. *Aust. J. Phys.* **1990**, *94*, 3962.
(87) Su, M.-C.; Parmenter, C. S. *Chem. Phys.* **1991**, *156*, 261.
(88) Cockett, M. C. R.; Okuyama, K.; Kimura, K. *J. Chem. Phys.* **1992**, *97*, 4679.
(89) Dyke, J. M.; Ozeki, H.; Takahashi, M.; Cockett, M. C. R.; Kimura, K. *J. Chem. Phys.* **1992**, *97*, 8926.
(90) Kim, H. Y.; Cole, M. W. *J. Chem. Phys.* **1989**, *90*, 6055.
(91) Dimopoulou-Rademann, O.; Even, U.; Amirav, A.; Jortner, J. *J. Phys. Chem.* **1988**, *92*, 5371.
(92) Mikami, N.; Sasaki, T.; Sato, S. *Chem. Phys. Lett.* **1991**, *180*, 431.
(93) Nakai, Y.; Ohashi, K.; Nishi, N. *J. Phys. Chem.* **1992**, *96*, 7873.

(94) Bieske, E. J.; Soliva, A. S.; Welker, M.; Maier, J. P. *J. Chem. Phys.* **1990**, *93*, 4477.
(95) Bieske, E. J.; Soliva, A. M.; Maier, J. P. *J. Chem. Phys.* **1991**, *94*, 4749.
(96) Bieske, E. J.; Soliva, A. M.; Friedmann, A.; Maier, J. P. *J. Chem. Phys.* **1992**, *96*, 28.
(97) Bieske, E. J.; Soliva, A. M.; Friedmann, A.; Maier, J. P. *J. Chem. Phys.* **1992**, *96*, 7535.
(98) Bieske, E. J.; Soliva, A. M.; Friedmann, A.; Maier, J. P. *J. Chem. Phys.* **1992**, *96*, 4035.
(99) David, D. E.; Magnera, T. F.; Tijan, R.; Stulik, D.; Michl, J. *Nucl. Instr. Meth.* **1986**, *B14*, 378.
(100) Lin, Y.; Heaven, M. C. *J. Chem. Phys.* **1991**, *94*, 5765.
(101) Soliva, A. M.; Bieske, E. J.; Maier, J. P. *Chem. Phys. Lett.* **1991**, *179*, 247.
(102) Knight, L. B.; Steadman, J.; Miller, P. K.; Bowman, D. E.; Davidson, E. R.; Feller, D. *J. Chem. Phys.* **1984**, *80*, 4593.
(103) Western, C. M.; Langridge-Smith, P. R. R.; Howard, B. J.; Novick, S. E. *Mol. Phys.* **1981**, *44*, 145.
(104) Menoux, V.; LeDoucen, R.; Hauesler, C.; Deroche, J. C. *Can. J. Phys.* **1984**, *62*, 322.
(105) Mills, P. D. A.; Western, C. M.; Howard, B. J. *J. Phys. Chem.* **1986**, *90*, 4961.
(106) Huber, K. P.; Herzberg, G. *Molecular Spectra and Molecular Structure IV. Constants of Diatomic Molecules*; van Nostrand Reinhold: New York, 1979.
(107) Kirchner, N. J.; Bowers, M. T. *J. Chem. Phys.* **1986**, *86*, 1301.
(108) Wright, L. R.; Borkman, R. F. *J. Chem. Phys.* **1982**, *77*, 1938.
(109) Elford, M. T.; Milloy, H. B. *Aust. J. Phys.* **1974**, *27*, 211.
(110) Elford, M. T. *J. Chem. Phys.* **1983**, *79*, 5951.
(111) Buehler, B.; Thalweiser, R.; Gerber, G. *Chem. Phys. Lett.* **1992**, *188*, 247–53.
(112) Johnsen, R.; Huang, C. M.; Biondi, M. A. *J. Chem. Phys.* **1976**, *65*, 1539.
(113) Bennett, S. L.; Field, F. H. *J. Am. Chem. Soc.* **1972**, *94*, 8669.
(114) Arifov, U. A.; Pozharov, S. L.; Chernov, I. G.; Mukhamediev, Z. A. *High Energy Chem. (U. S. S. R.)* **1971**, *5*, 69.
(115) Gerlich, D.; Horning, S. *Chem. Rev.* **1992**, *92*, 1509.
(116) Hirao, K.; Yamabe, S. *Chem. Phys.* **1983**, *80*, 237.
(117) Huber, H. *Chem. Phys. Lett.* **1980**, *70*, 353.
(118) Huber, H. *J. Mol. Struct.* **1985**, *121*, 281.
(119) Yamaguchi, Y.; Gaw, J. F.; Schaefer, H. F., III. *J. Chem. Phys.* **1983**, *78*, 4074.
(120) Yamaguchi, Y.; Gaw, J. F.; Remmington, R. B.; Schaefer, H. F., III. *J. Chem. Phys.* **1987**, *86*, 5072.
(121) Farizon, M.; Chermette, H.; Farizon-Mazuy, B. *J. Chem. Phys.* **1991**, *696*, 1325.
(122) Okumura, M.; Yeh, L. I.; Lee, Y. T. *J. Chem. Phys.* **1985**, *83*, 3705.
(123) Okumura, M.; Yeh, L. I.; Lee, Y. T. *J. Chem. Phys.* **1988**, *88*, 79.
(124) Bae, Y. K. *Chem. Phys. Lett.* **1991**, *180*, 179.
(125) Searcy, J. Q.; Fenn, J. B. *J. Chem. Phys.* **1974**, *61*, 5282.
(126) Daly, N. R. *Rev. Sci. Instr.* **1960**, *31*, 264.
(127) Bedford, D. K.; Smith, D. *Int. J. Mass Spectrom. Ion Processes* **1990**, *98*, 179.
(128) Bogey, M.; Bolvin, H.; Demuynck, C.; Destombes, J. L. *Phys. Rev. Lett.* **1987**, *58*, 988.
(129) Bogey, M.; Bolvin, H.; Demuynck, C.; Destombes, J. L.; Eijck, B. P. V. *J. Chem. Phys.* **1988**, *88*, 4120.
(130) Simandiras, E. D.; Gaw, J. F.; Handy, N. C. *Chem. Phys. Lett.* **1987**, *141*, 166.
(131) Raynor, S.; Herschbach, D. R. *J. Phys. Chem.* **1983**, *87*, 289.
(132) Kojima, T. M.; Kobyashi, N.; Kaneko, Y. *Z. Phys. D.* **1992**, *23*, 181.
(133) Ferguson, E. E.; Fehsenfeld, F. C.; Albritton, D. L. In *Gas Phase Ion Chemistry*; Bowers, M. T., Ed.; Academic: New York, 1979.
(134) Begemann, M. H.; Gudeman, C. S.; Pfaaf, J.; Saykally, R. J. *Phys. Rev. Lett.* **1983**, *51*, 554.
(135) Begemann, M. H.; Saykally, R. J. *J. Chem. Phys.* **1985**, *82*, 3570.
(136) Liu, D.; Haese, N. H.; Oka, T. *J. Chem. Phys.* **1985**, *82*, 5368.
(137) Liu, D.; Oka, T.; Sears, T. J. *J. Chem. Phys.* **1986**, *84*, 1312.
(138) Schwarz, H. A. *J. Chem. Phys.* **1977**, *67*, 5525.
(139) Kebarle, P.; Searles, S. K.; Zolla, A.; Scarborough, J.; Arshadi, M. *J. Am. Chem. Soc.* **1967**, *89*, 6393.
(140) Yeh, L. I.; Okumura, M.; Myers, J. D.; Price, J. M.; Lee, Y. T. *J. Chem. Phys.* **1989**, *91*, 7319.
(141) Okumura, M.; Yeh, L. I.; Myers, J. D.; Lee, Y. T. *J. Chem. Phys.* **1986**, *85*, 2328.
(142) Okumura, M.; Yeh, L. I.; Myers, J. D.; Lee, Y. T. *J. Phys. Chem.* **1990**, *94*, 3416.
(143) Lias, S. G.; Liebman, J. F.; Levin, R. D. *J. Phys. Chem. Ref. Data* **1984**, *13*, 695.
(144) Hogg, A. M.; Haynes, R. M.; Kebarle, P. *J. Am. Chem. Soc.* **1966**, *88*, 28.
(145) Searles, S. K.; Kebarle, P. *J. Phys. Chem.* **1968**, *72*, 742.
(146) Schwarz, H. A. *J. Chem. Phys.* **1980**, *72*, 284.
(147) Crofton, M. W.; Oka, T. *J. Chem. Phys.* **1983**, *79*, 3157.
(148) Crofton, M. W.; Oka, T. *J. Chem. Phys.* **1987**, *86*, 5983.
(149) Schafer, E.; Saykally, R. *J. Chem. Phys.* **1984**, *80*, 3969.
(150) Price, J. M.; Crofton, M. W.; Lee, Y. T. *J. Chem. Phys.* **1989**, *91*, 2749.
(151) Price, J. M.; Crofton, M. W.; Lee, Y. T. *J. Phys. Chem.* **1991**, *95*, 2182.
(152) Yeh, L. I.; Price, J. M.; Lee, Y. T. *J. Am. Chem. Soc.* **1989**, *111*, 5597.
(153) Hiraoka, K.; Kebarle, P. *J. Am. Chem. Soc.* **1976**, *98*, 6119.
(154) Yeh, C. Y.; Willey, K. F.; Robbins, D. L.; Duncan, M. A. *J. Phys. Chem.* **1992**, *96*, 4824.
(155) Willey, K. F.; Yeh, C. S.; Robbins, D. L.; Duncan, M. A. *Chem. Phys. Lett.* **1992**, *92*, 179.
(156) Willey, K. F.; Yeh, C. S.; Robbins, D. L.; Pilgrim, J. S.; Duncan, M. A. *J. Chem. Phys.* **1992**, *97*, 8886.
(157) Sodupe, M.; Bauschlicher, C. W.; Partridge, H. *Chem. Phys. Lett.* **1992**, *192*, 185.
(158) Yeh, C. S.; Willey, K. F.; Robbins, D. L.; Pilgrim, J. S.; Duncan, M. A. *Chem. Phys. Lett.* **1992**, *196*, 233.
(159) Sodupe, M.; Bauschlicher, C. W. *Chem. Phys. Lett.* **1992**, *195*, 494.
(160) Misaizu, F.; Sanekataa, M.; Tsukamoto, K.; Fuke, K.; Iwata, S. *J. Phys. Chem.* **1992**, *96*, 8259.
(161) Shen, M. H.; Winniczek, J. W.; Farrar, J. M. *J. Phys. Chem.* **1987**, *91*, 6447.
(162) Shen, M. H.; Farrar, J. M. *J. Phys. Chem.* **1989**, *93*, 4386.
(163) Shen, M. H.; Farrar, J. M. *J. Chem. Phys.* **1991**, *94*, 3322.
(164) Liu, W.; Lisy, J. M. *J. Chem. Phys.* **1988**, *89*, 605.
(165) Draves, J. A.; Luthey-Schulten, Z.; Liu, W.-L.; Lisy, J. M. *J. Chem. Phys.* **1990**, *93*, 4589.
(166) Selegue, T. J.; Lisy, J. M. *J. Phys. Chem.* **1992**, *96*, 4143.
(167) Lessen, D.; Brucat, P. J. *J. Chem. Phys.* **1989**, *91*, 4522.
(168) Lessen, D. E.; Asher, R. L.; Brucat, P. J. *J. Chem. Phys.* **1990**, *93*, 6102.
(169) Lessen, D. E.; Asher, R. L.; Brucat, P. J. *Chem. Phys. Lett.* **1991**, *177*, 380.
(170) Lessen, D.; Brucat, P. J. *Chem. Phys. Lett.* **1988**, *152*, 473.
(171) Lessen, D.; Brucat, P. J. *J. Chem. Phys.* **1989**, *90*, 6296.
(172) Lessen, D.; Asher, R. L.; Brucat, P. J. *Int. J. Mass Spectr. Ion Processes* **1990**, *102*, 331.
(173) Takebe, M. J. *J. Chem. Phys.* **1983**, *78*, 4597.
(174) Bottner, E.; Dimpl, W. L.; Ross, U.; Toennies, J. P. *Chem. Phys. Lett.* **1975**, *32*, 197.
(175) Gatland, I. R. *J. Chem. Phys.* **1981**, *77*, 3983.
(176) Polak-Dingels, P.; Rajan, M. S.; Gislason, E. A. *J. Chem. Phys.* **1982**, *77*, 3983.
(177) Powers, T. R.; Cross, R. J. *J. Chem. Phys.* **1973**, *58*, 626.
(178) Lamm, D. R.; Thackston, M. G.; Eisele, F. E.; Ellis, W. H.; Twist, J. R.; Pope, W. M.; Gatland, I. R.; McDaniel, E. W. *J. Chem. Phys.* **1981**, *74*, 3042.
(179) Shamp, H. W.; Mason, E. A. *Ann. Phys.* **1958**, *4*, 233.
(180) Skullerud, H. J. *J. Phys. B* **1973**, *6*, 918.
(181) Lessen, D.; Brucat, P. J. *Chem. Phys. Lett.* **1988**, *149*, 10.
(182) DeLuca, M. J.; Han, C.-C.; Johnson, M. A. *J. Chem. Phys.* **1990**, *93*, 268.
(183) Campagnola, P. J.; Posey, L. A.; Johnston, M. A. *J. Chem. Phys.* **1991**, *95*, 7998.
(184) Posey, L. A.; Johnson, M. A. *J. Chem. Phys.* **1988**, *88*, 5383.
(185) Alexander, M. L.; Levinger, N. E.; Johnson, M. A.; Ray, D.; Lineberger, W. C. *J. Chem. Phys.* **1988**, *88*, 6200.
(186) Ray, D.; Levinger, N. E.; Papanikolas, J. M.; Lineberger, W. C. *J. Chem. Phys.* **1989**, *91*, 6533.
(187) Deluca, M. J.; Johnson, M. A. *Chem. Phys. Lett.* **1988**, *152*, 67.
(188) Coe, J. V.; Snodgrass, J. T.; Freidhoff, C. B.; McHugh, K. M.; Bowen, K. H. *J. Chem. Phys.* **1987**, *87*, 4302.
(189) DeLuca, M. J.; Niu, B.; Johnson, M. A. *J. Chem. Phys.* **1988**, *88*, 5857.
(190) Nagata, T.; Yoshida, H.; Kondow, T. *Chem. Phys. Lett.* **1992**, *199*, 205.
(191) Arnold, D. W.; Bradforth, S. E.; Kim, E. H.; Neumark, D. M. *J. Chem. Phys.* **1992**, *97*, 9468.
(192) Markovich, G.; Giniger, R.; Levin, M.; Cheshnovsky, O. *Z. Phys. D.* **1991**, *20*, 69.